NACA RM L58E21

NACA

RESEARCH MEMORANDUM

AERODYNAMIC CHARACTERISTICS AT MACH NUMBERS 2.36 AND 2.87 OF AN AIRPLANE CONFIGURATION HAVING A CAMBERED ARROW WING WITH A 75° SWEPT LEADING EDGE

By Joseph M. Hallissy, Jr., and Dennis F. Hasson

Langley Aeronautical Laboratory
Langley Field, Va.

NATIONAL ADVISORY COMMITTEE
FOR AERONAUTICS
WASHINGTON

August 4, 1958
Declassified January 12, 1961

NATIONAL ADVISORY COMMITTEE FOR AERONAUTICS

RESEARCH MEMORANDUM

AERODYNAMIC CHARACTERISTICS AT MACH NUMBERS 2.36 AND 2.87 OF AN AIRPLANE CONFIGURATION HAVING A CAMBERED ARROW WING WITH A 75° SWEPT LEADING EDGE*

By Joseph M. Hallissy, Jr., and Dennis F. Hasson

SUMMARY

An investigation has been conducted to determine the performance and static stability characteristics of a model of a long-range bomber intended to cruise at Mach number 3.0. This configuration utilized a wing having a 75° sweptback leading edge and having camber and twist to give maximum lift-drag ratio at a lift coefficient of 0.1. The aspect ratio was 1.79 and the taper ratio 0. Wing thickness in sections normal to the leading edge varied between 8 and 14 percent chord. Configurations tested included the wing alone and two complete flying-wing type configurations, one having six separate underslung engine pods and the other having a clustered-engine installation with common inlet ducting.

Tests were conducted at Mach numbers 2.36 and 2.87, through a range of angle of attack from -4° to 10°. The Reynolds number based on mean aerodynamic chord was about 4.2×10^6 for most tests. Maximum lift-drag ratios at Mach number 2.87 were 6.8 for the wing alone, 6.2 for the complete configuration having six underslung engine pods, and 5.2 for the complete configuration with the clustered-engine arrangement. These results are below the anticipated performance, probably because of unfavorable flow conditions on the upper surface. All configurations were longitudinally stable and trimmed near the design lift coefficient. The two complete configurations, which had vertical half-delta fins mounted on the wings near the tips, were directionally stable.

INTRODUCTION

In the search for an airplane configuration which has a lift-drag ratio at Mach number 3.0 high enough to be useful as a long-range all-supersonic bomber, one possibility to be considered is a configuration incorporating a highly swept wing with subsonic leading edges. Linearized

*Title, Unclassified.

theory indicates that the drag due to lift would be low for such a wing. Furthermore, the possibility exists that, when the wing is cambered, the configuration may be made stable and trimmed for the design load distribution. This arrangement would permit the elimination of a horizontal stabilizer and the attendant trim and skin-friction drag. In addition, if the required airplane volume is incorporated in the wing, it would be possible to eliminate or minimize the fuselage volume with a further reduction in skin-friction drag. Accordingly, as one part of a Langley laboratory research program on supersonic-bomber designs (refs. 1 and 2), a configuration with leading edges swept 75° and with the design camber and twist condition at a lift coefficient of 0.1 was laid out, and a wind-tunnel test program was planned to determine whether the high lift-drag ratios were attainable experimentally and to investigate the static stability characteristics of such a wing.

The results obtained in the wind-tunnel tests at Mach numbers 2.36 and 2.87 for several configurations utilizing this wing, including results on the wing alone are presented.

SYMBOLS

The force and moment coefficient data are presented by using the system of axes shown in figure 1. The reference center for the moment data is at the apex of the wing trailing edge.

b	wing span, in.
$\bar{c}$	wing mean aerodynamic chord, in.
C_D'	drag coefficient, $\frac{\text{Drag}}{qS}$
$C_{D,min}'$	minimum drag coefficient
$C_{D,o}'$	drag coefficient at zero lift
$\Delta C_D'$	drag-coefficient increment used in correcting measured drag coefficient
C_L	lift coefficient, $\frac{\text{Lift}}{qS}$
C_m	pitching-moment coefficient, $\frac{\text{Pitching moment}}{qS\bar{c}}$
C_l	rolling-moment coefficient, $\frac{\text{Rolling moment}}{qSb}$

C_n yawing-moment coefficient, $\frac{\text{Yawing moment}}{qSb}$

C_Y lateral-force coefficient, $\frac{\text{Lateral force}}{qS}$

C_p pressure coefficient, $\frac{p_l - p}{q}$

C_{L_α} lift-curve slope, per degree

$C_{l_\beta} = \frac{\Delta C_l}{\Delta \beta}$, calculated as $\frac{(C_l)_{\beta=4^o} - (C_l)_{\beta=-4^o}}{8}$ per deg

$C_{n_\beta} = \frac{\Delta C_n}{\Delta \beta}$, calculated as $\frac{(C_n)_{\beta=4^o} - (C_n)_{\beta=-4^o}}{8}$ per deg

$C_{Y_\beta} = \frac{\Delta C_Y}{\Delta \beta}$, calculated as $\frac{(C_Y)_{\beta=4^o} - (C_Y)_{\beta=-4^o}}{8}$ per deg

M free-stream Mach number

p_l local static pressure, lb/sq ft

p free-stream static pressure, lb/sq ft

q free-stream dynamic pressure, $0.7pM^2$, lb/sq ft

S total wing area, (total area is used in computing force and moment coefficients for all configurations, including the tips-off configuration), sq ft

x' distance along wing leading edge from the leading edge apex, in.

y' distance from wing leading edge measured normal to the leading edge, in.

z_u upper-surface ordinate, measured normal to wing reference plane, in.

z_l lower surface ordinate, measured normal to wing reference plane, in.

α angle of attack of the balance axis (balance axis is 2^o noseup relative to the wing reference plane), deg

β angle of sideslip, deg

δ_e angular deflection of wing tips about their hinge lines, positive trailing edge down, deg

δ_r angular deflection of rudders, positive trailing edge left, deg

Subscripts:

L left wing

R right wing

APPARATUS AND METHODS

Tunnel

The tests were conducted in the low Mach number test section of the Langley Unitary Plan Wind Tunnel, which is a variable-pressure, continuous, return-flow tunnel. The test section is 4 feet square and approximately 7 feet in length. The nozzle leading to the test section is of the asymmetric sliding-block type. The tunnel is equipped with a central support system which permits remote control of the angles of attack and sideslip of a sting-mounted model.

Model and Instrumentation

The wing used in this investigation was designed by C. E. Brown and F. E. McLean of the Langley Aeronautical Laboratory. The plan form of the wing was selected on the basis of indications by the linear theory that at supersonic speeds lift can be carried efficiently by an arrow wing having subsonic leading edges (ref. 3, p. 202, fig. A,14m). The wing was cambered and twisted to provide a design lift coefficient of 0.1 at Mach number 3.0 by using the superposition method of references 4 and 5 and imposing the condition that the drag due to lift be a minimum for the plan form selected. A 63A thickness distribution, with the sections normal to the leading edge, was then wrapped symmetrically around the mean camber surface. The overall thickness was determined by approximate volume requirements for a long-range bomber design, rather than by structural requirements. The spanwise thickness distribution and the resulting longitudinal distribution of cross-section areas are shown in figure 2. The ordinates of the upper and lower surfaces of the wing are given in table I. The photographs of a wood mock-up of the wing presented as figure 3 are presented to help in visualizing the surface contours.

The wing was intended to be stable and to trim at the design point without the use of auxiliary longitudinal stabilizing surfaces; therefore, the concept for the complete airplane was that of a flying wing having little or no fuselage and with all required internal volume provided by the wing. Three-view drawings of several of the configurations investigated are shown in figure 4 and additional geometric details are listed in table II. Configurations tested were the wing alone (with the minimum center body required to enclose the balance), the wing alone with movable tips off, the wing with a rectangular body fairing on the upper surface, the wing with two half-delta vertical fins mounted on the upper surfaces, and two complete airplane configurations with simulated engine installation and vertical fins. One of these configurations had six underslung single pods and a pair of half-delta fins mounted on the upper surface (fig. 4(b)). The other had a cluster of six engines with a common underslung inlet and ducting and half-delta fins on both the upper and lower surfaces (fig. 4(c)). The same wing (fig. 1(a)) was used for each configuration, the differences among the configurations being in the engine installation, vertical fins, and center body. The photographs of figure 5 show some of the test configurations.

The vertical fins and pods were positioned so as to be aligned with the calculated local flow at the design lifting condition. Inlet geometry for both types of simulated engine installation was fixed at the Mach number 3.0 condition, and it was determined that flow in the inlets was supersonic at almost all test conditions, the only exception being that the outboard pods at large negative attitudes may not have been started because of the large flow angularity.

The size of the engine exits was such that the exit flow was choked throughout the test speed range. In order to determine the internal drag, the exit pressures were measured by either a total-pressure tube just inside the exit (in the case of the clustered engine installation) or a flush static-pressure tube in the straight exit pipe (in the case of the six-pod engine installation).

Forces and moments were obtained on a six-component electrical strain-gage balance mounted within the model. The model-balance assembly was sting-mounted from the tunnel central-support system.

Tests

Most of the tests were conducted at the conditions indicated in the following list:

Mach number	2.36	2.87
Reynolds number (based on $\bar{c}$)	4.3×10^6	4.2×10^6
Stagnation pressure, atm	0.93	1.21
Dynamic pressure, lb/sq ft	560	490
Stagnation temperature, $^{\circ}F$	150	150
Dewpoint, $^{\circ}F$	< -30	< -30
Angles of attack, deg	-4 to +10	-4 to +10
Angles of sideslip, deg	-4, 0, 4	-4, 0, 4
Transition	Fixed	Fixed

The transition strips consisted of bands of sand 3/32 inch wide sparsely applied to the surfaces with a plastic spray. The grain size was 0.010 inch to 0.013 inch with the strip applied at 5 percent of the local streamwise chord on the wing and at 8.5 percent of the chord on the fins. A few data were also obtained at Reynolds numbers of 2.5×10^6, 6.3×10^6, and 8.2×10^6, and some tests were made with natural transition.

Additional tests were required for pressure measurements needed to evaluate the internal drag and base pressures. In order to provide some insight concerning air-flow conditions on the wing, pressure orifices were installed and a limited amount of pressure data was obtained on the wing alone.

A flow-visualization technique which utilized a fluorescent oil painted on the wing surface was also employed. The photographs of the wing surface, made with the tunnel in operation, indicate the areas of attached and separated flow as well as the air-flow direction on the surface. The model was translated forward and rearward in the test section to obtain full photographic coverage of the wing, and the resulting prints were pieced together to form a composite.

Corrections and Accuracy

The maximum deviation of local Mach number in the part of the tunnel occupied by the model is ±0.015 from the average value given. The pressure gradients are sufficiently small that no buoyancy correction is required.

The average angularity of the flow in the region of the model was determined by comparing inverted and upright runs and the angle of attack corrected accordingly. The angles of attack and sideslip have been corrected for balance-sting deflection and are accurate to within $\pm 0.1^{\circ}$.

The internal drag has been subtracted from the measured drag, and the data have also been adjusted to the condition of free-stream static pressure on the model base and engine bases. No corrections or adjustments

have been made relative to the boundary-layer diverter drag of the clustered-engine configuration.

Based upon balance accuracy and repeatability of data, it is estimated that the coefficients are accurate within the following limits:

C_L	±0.003
C_D'	±0.0005
C_m	±0.0005
C_l	±0.0003
C_n	±0.0003
C_Y	±0.002
C_p	±0.005

PRESENTATION OF RESULTS

The results of this investigation are presented in the following figures:

	Figure
Schlieren photographs of the model	6
Composite of oil-film flow photographs of wing alone	7
Pressure distribution on wing alone at angles of attack near design condition	8
Base, chamber, and internal drag coefficients for various model configurations	9
Boundary-layer-diverter pressures for clustered engine configuration	10
Longitudinal characteristics of the various model configurations	11
Effects of transition at two Reynolds numbers on longitudinal characteristics of wing alone at M = 2.87	12
Variation of $C_{D,min}'$ with Reynolds number for fixed and natural transition on wing alone at a Mach number of 2.87	13
Summary of longitudinal characteristics of several model configurations	14
Lateral characteristics of various model configurations at Mach number 2.87	15
Sideslip derivatives for several model configurations at Mach number 2.87	16

SUMMARY OF RESULTS

Performance

At Mach number 2.87, which is near the design speed, the maximum lift-drag ratio for the wing alone is 6.8 (fig. 14). For the complete airplane configuration with six underslung pods and upper surface fins, the value of $(L/D)_{max}$ is 6.2, and for the complete configuration with the clustered engine installation and both upper and lower surface fins the value $(L/D)_{max}$ is 5.2. These numbers are appreciably below the anticipated levels, and it will be worthwhile to consider briefly the cause of this difference.

Figure 11(b) compares the experimental data for the wing-alone configuration with the theoretical longitudinal characteristics obtained in the design calculations for $M = 3.0$. The drag-coefficient polars indicate that, although a low level of minimum drag was achieved, the drag due to lift for $M = 2.87$ was much higher than the calculated result for $M = 3.00$. Furthermore, theory indicates that the lift-curve slope at Mach number 3.00 should be about 0.0253, but the present test results at $M = 2.87$ were about 13 percent below this value for lift coefficients up to 0.1. From these results, it is apparent that the wing is not achieving its intended performance. It is believed that this deficiency is due to unfavorable flow conditions on the upper surface. The oil-film flow photographs of figure 7 indicate a region of attached flow over the forward portion of the wing. Behind this region the flow is separated from the surface, as is indicated by the lack of scrubbing and the erratic oil-flow paths. On each of the pressure distributions of figure 8 is shown the level of pressure coefficient which corresponds to $M = 1.0$ in the direction normal to the leading edge, and it can be seen that this value of the pressure coefficient is exceeded at every station. The flow separation is therefore probably associated with the existence of supercritical flow (in a direction normal to the leading edge) and attendant shock waves on the upper surface. The rectangular body fairing, shown in figures 4(a) and 5(b), was added to the upper surface in an effort to move the wing shock wave nearer the leading edge and thereby to weaken the shock wave and reduce the amount of separation. No conclusive visual evidence of flow changes were obtained, but force data (fig. 11(c)) shows a reduction of maximum lift-drag ratio to 6.4, so that any gains were more than offset by a loss of lift or an increase of drag, or both.

Although the performance of the best complete configuration of this investigation is below its estimated design capability, it should be pointed out that the maximum lift-drag ratios obtained are comparable with those obtained on other configurations intended for the long-range airplane (refs. 1 and 2).

Longitudinal Stability

For the center-of-gravity position used in the data reduction, all configurations (except the configuration with wing tips off) were longitudinally stable throughout the lift and Mach number range of the tests. The stability for the wing alone was not as great, however, as the calculated value (fig. 11(b)), the calculated aerodynamic center being about $0.12\bar{c}$ aft of the experimental location. All configurations showed reductions of stability above $C_L = 0.2$, but none became unstable within the test range.

The effectiveness of the tips as a longitudinal trim device is indicated by comparing figures 11(g) and 11(h). At $M = 2.87$ a tip deflection of -5° increased the trim lift coefficient from 0.090 to 0.155.

Lateral and Directional Stability

Tests to determine effects of sideslip, rudder deflection, and opposite tip deflection were made only at $M = 2.87$. All configurations had positive effective dihedral, $-C_{l_\beta}$, throughout the angle-of-attack range (fig. 15), although the location and amount of fin and nacelle area affected the magnitude, as would be expected.

The basic wing-alone configuration had neutral directional stability throughout the angle-of-attack range, so that the addition of fins and nacelles always resulted in positive C_{n_β}, figure 16. Variations with angle of attack were about as might be anticipated: a rather severe decrease as α increased when only the upper-surface fins are mounted, but flatter curves for the other configurations having nacelles or fins below the wing.

Langley Aeronautical Laboratory,
National Advisory Committee for Aeronautics,
Langley Field, Va., May 7, 1958.

REFERENCES

1. Kelly, Thomas C., Carmel, Melvin M., and Gregory, Donald T.: An Exploratory Investigation at Mach Numbers of 2.50 and 2.87 of a Canard Bomber-Type Configuration Designed for Supersonic Cruise Flight. NACA RM L58B28, 1958.

2. Church, James D., Hayes, William C., Jr., and Sleeman, William C.: Investigation of Aerodynamic Characteristics of an Airplane Configuration Having Tail Surfaces Outboard of the Wing Tips at Mach Numbers of 2.30, 2.97, and 3.51. NACA RM L58C25, 1958.

3. Jones, Robert T., and Cohen, Doris: Aerodynamic Wings at High Speeds. Aerodynamic Components of Aircraft at High Speeds, vol VII of High Speed Aerodynamics and Jet Propulsion, sec. A, A. F. Donovan and H. R. Lawrence, eds., Princeton Univ. Press, 1957, pp. 3-243.

4. Tucker, Warren A.: A Method for the Design of Sweptback Wings Warped to Produce Specific Flight Characteristics at Supersonic Speeds. NACA Rep. 1226, 1955. (Supersedes NACA RM L51F08.)

5. Grant, Frederick C.: The Proper Combination of Lift Loadings for Least Drag on a Supersonic Wing. NACA Rep. 1275, 1956. (Supersedes NACA TN 3533.)

TABLE I.- WING ORDINATES

[All dimensions are in inches. Ordinates to the upper and lower surfaces, z_u and z_l, are measured normal to the wing reference plane which is parallel to the free stream when the wing is at the design attitude. Ordinates are positive upward.]

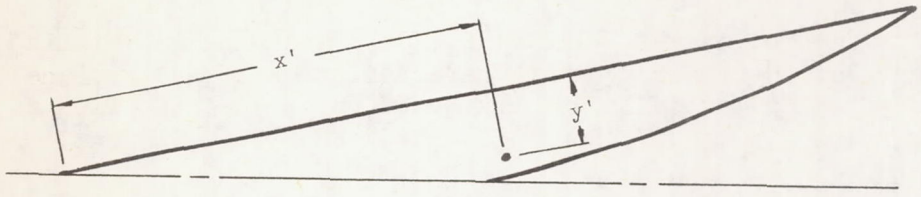

y'	z_u	z_l
x' = 0		
0.000	3.045	3.045
x' = 3.0		
0.000	1.149	1.149
.015	1.209	1.118
.045	1.268	1.122
.075	1.319	1.131
.152	1.416	1.163
.230	1.518	1.203
.309	1.617	1.254
.389	1.710	1.308
.470	1.814	1.371
.551	1.926	1.443
.635	2.046	1.538
.719	2.198	1.649
.804	2.393	1.808
x' = 6.0		
0.000	0.594	0.594
.030	.684	.557
.060	.732	.552
.120	.797	.558
.152	.833	.563
.305	.962	.581
.381	1.019	.591
.537	1.116	.614
.617	1.163	.626
.696	1.206	.636
.857	1.287	.662
1.020	1.367	.684
1.101	1.406	.698
1.185	1.442	.710
1.352	1.500	.731
1.608	1.568	.744

y'	z_u	z_l
x' = 9.0		
0.000	0.272	0.272
.045	.386	.231
.090	.438	.221
.135	.474	.219
.227	.548	.210
.341	.614	.203
.572	.725	.188
.689	.767	.182
1.044	.872	.167
1.164	.899	.162
1.286	.926	.155
1.529	.960	.135
1.653	.968	.120
1.902	.951	.065
2.028	.917	.010
2.154	.864	-.065
2.283	.786	-.155
2.412	.698	-.255
x' = 12.0		
0.000	0.125	0.125
.060	.239	.069
.120	.290	.051
.240	.366	.020
.302	.398	.008
.455	.458	-.020
.762	.537	-.069
.918	.566	-.096
1.076	.590	-.123
1.391	.612	-.179
1.553	.620	-.207
1.713	.621	-.234
2.039	.609	-.296
2.204	.596	-.329
2.537	.536	-.419
2.705	.480	-.480
3.044	.284	-.705
3.215	.119	-.863

y'	z_u	z_l
x' = 15.0		
0.000	0.081	0.081
.075	.201	.014
.150	.251	-.012
.227	.287	-.035
.378	.344	-.075
.569	.390	-.125
.761	.419	-.174
1.148	.429	-.276
1.344	.422	-.327
1.542	.410	-.380
1.940	.372	-.488
2.142	.342	-.540
2.345	.308	-.596
2.754	.224	-.707
2.961	.173	-.765
3.170	.113	-.825
3.591	-.053	-.975
4.019	-.322	-1.208
x' = 18.0		
0.000	0.096	0.096
.090	.225	.030
.180	.282	-.002
.270	.320	-.026
.362	.345	-.050
.683	.395	-.150
.912	.392	-.231
1.377	.344	-.390
1.613	.309	-.471
1.850	.266	-.551
2.328	.156	-.704
2.570	.098	-.780
2.813	.029	-.858
3.305	-.131	-1.010
3.554	-.219	-1.086
3.803	-.317	-1.164
4.565	-.641	-1.395
4.823	-.756	-1.470

TABLE I.- WING ORDINATES - Continued

y'	z_u	z_l
x' = 21.0		
0.000	0.109	0.109
.105	.250	.039
.210	.315	.010
.317	.352	-.014
.423	.381	-.041
.528	.400	-.068
1.065	.409	-.239
1.335	.375	-.341
1.881	.247	-.553
2.159	.169	-.661
2.717	-.020	-.874
2.999	-.119	-.977
3.282	-.227	-1.076
3.857	-.458	-1.267
4.146	-.580	-1.346
4.733	-.824	-1.489
5.327	-1.069	-1.621
5.627	-1.186	-1.682
x' = 24.0		
0.000	0.117	0.117
.120	.278	.041
.240	.338	.014
.360	.384	-.014
.483	.419	-.044
.605	.441	-.072
.909	.462	-.156
1.526	.398	-.360
1.838	.324	-.480
2.151	.224	-.611
2.466	.108	-.749
2.784	-.021	-.882
3.104	-.161	-1.013
3.752	-.462	-1.260
4.077	-.615	-1.373
4.407	-.767	-1.475
5.072	-1.068	-1.638
5.408	-1.209	-1.704
6.087	-1.470	-1.805
6.431	-1.568	-1.832

y'	z_u	z_l
x' = 27.0		
0.000	0.118	0.118
.135	.293	.038
.270	.368	.004
.407	.419	-.028
.680	.484	-.093
1.023	.502	-.180
1.368	.478	-.285
1.716	.416	-.400
2.067	.334	-.526
2.420	.220	-.661
2.775	.074	-.805
3.492	-.289	-1.114
3.855	-.489	-1.272
4.587	-.903	-1.552
5.331	-1.288	-1.762
5.706	-1.453	-1.837
6.084	-1.591	-1.882
6.465	-1.702	-1.900
6.849	-1.789	-1.894
7.234	-1.858	-1.867
x' = 30.0		
0.000	0.113	0.113
.150	.311	.020
.300	.389	-.013
.452	.446	-.050
.603	.486	-.081
1.137	.536	-.210
1.521	.504	-.320
1.907	.437	-.444
2.297	.336	-.569
2.688	.200	-.707
3.083	.032	-.854
3.480	-.179	-1.014
3.881	-.414	-1.185
4.283	-.662	-1.346
4.689	-.921	-1.514
5.097	-1.184	-1.670
5.508	-1.433	-1.805
5.922	-1.629	-1.895
6.341	-1.788	-1.952
6.930	-1.989	-1.992

y'	z_u	z_l
x' = 33.0		
0.000	0.101	0.101
.165	.315	.003
.332	.401	-.031
.497	.459	-.066
.663	.501	-.099
.831	.528	-.135
1.250	.549	-.228
1.673	.512	-.338
2.097	.432	-.456
2.526	.312	-.585
2.957	.152	-.719
3.392	-.045	-.863
3.828	-.288	-1.022
4.268	-.560	-1.191
4.712	-.855	-1.371
5.157	-1.154	-1.554
5.607	-1.461	-1.739
6.059	-1.757	-1.905
6.515	-1.998	-2.021
6.602	-2.030	-2.033
x' = 36.0		
0.000	0.085	0.085
.180	.308	-.015
.362	.400	-.053
.542	.463	-.083
.725	.508	-.118
.906	.537	-.151
1.364	.558	-.242
1.824	.505	-.347
2.289	.405	-.461
2.756	.268	-.583
3.225	.084	-.710
3.699	-.146	-.848
4.176	-.422	-1.004
4.656	-.725	-1.171
5.139	-1.039	-1.357
5.627	-1.384	-1.562
6.117	-1.730	-1.775
6.255	-1.835	-1.835

TABLE I.- WING ORDINATES - Concluded

y'	z_u	z_l
x' = 39.0		
0.000	0.067	0.067
.195	.294	-.030
.392	.391	-.063
.588	.454	-.093
.785	.499	-.122
.981	.526	-.152
1.478	.544	-.238
1.977	.486	-.334
2.480	.363	-.439
2.985	.204	-.548
3.495	-.008	-.665
4.008	-.268	-.800
4.524	-.572	-.958
5.045	-.899	-1.135
5.568	-1.235	-1.327
5.877	-1.444	-1.447
x' = 42.0		
0.000	0.046	0.046
.210	.277	-.044
.422	.380	-.077
.633	.445	-.106
.845	.493	-.131
1.058	.520	-.159
1.592	.529	-.231
2.129	.455	-.313
2.670	.314	-.402
3.215	.127	-.496
3.764	-.110	-.595
4.316	-.399	-.726
4.872	-.724	-.894
5.432	-1.072	-1.081
5.456	-1.086	-1.089
x' = 45.0		
0.000	0.020	0.020
.225	.254	-.063
.452	.356	-.088
.678	.420	-.109
.905	.464	-.129
1.133	.492	-.147
1.704	.500	-.203
2.280	.402	-.266
2.861	.240	-.332
3.444	.024	-.407
4.032	-.231	-.501
4.625	-.534	-.632
4.967	-.716	-.719

y'	z_u	z_l
x' = 48.0		
0.000	-0.009	-0.009
.240	.216	-.074
.482	.310	-.089
.723	.376	-.101
.966	.418	-.111
1.208	.439	-.120
1.818	.435	-.146
2.433	.316	-.180
3.051	.132	-.224
3.674	-.098	-.289
4.301	-.359	-.382
4.380	-.379	-.382
x' = 51.0		
0.000	-0.038	-0.038
.255	.164	-.074
.512	.248	-.076
.768	.310	-.073
1.026	.347	-.068
1.284	.362	-.062
1.932	.335	-.043
2.585	.200	-.055
3.242	-.005	-.101
3.641	-.131	-.134
x' = 54.0		
0.000	-0.075	-0.075
.270	.100	-.078
.542	.175	-.056
.813	.225	-.035
1.086	.250	-.011
1.359	.253	.015
2.046	.207	.087
2.634	.076	.076
x' = 57.0		
0.000	-0.118	-0.118
.285	.011	-.069
.572	.059	-.007
.858	.072	.053
.975	.075	.075
x' = 57.956		
0.000	-0.134	-0.134

TABLE II.- GEOMETRIC CHARACTERISTICS OF THE MODELS

[Stations are inches rearward of wing-leading-edge apex]

Center-of-gravity location:	
Longitudinal	Station 27.98
Distance below the wing reference plane, in.	1.86
Wing:	
Area, total including tips, sq ft	3.490
Span, in.	30.0
Aspect ratio	1.79
Taper ratio	0
Sweepback of leading edge, deg	75
Total length in streamwise direction, nose to wing tip, in.	55.97
Root chord, in.	27.98
Mean aerodynamic chord, in.	20.43
Mean-aerodynamic-chord lateral location, in.	5.49
Area outside of the upper vertical fins (or movable tip area), total for both sides, sq ft	0.562
Vertical fins (applies to either upper or lower except as noted):	
Area, each upper fin, sq ft	0.283
Area, each lower fin, sq ft	0.255
Height, in.	6.859
Taper ratio	0
Sweepback of the leading edge relative to the local wing chord, deg	30.0
Mean aerodynamic chord, in.	7.92
Root chord, in.	11.88
Longitudinal location of root chord midpoint	Station 43.39
Lateral location of root chord midpoint from plane of symmetry, in.	9.564
Toe-in of lower fins, deg	4.50
Toe-in of upper fins, deg	-4.50
Airfoil section parallel to local wing chord	5-percent-thick circular arc
Circular fuselage (used with wing alone configuration and with six-pod configuration):	
Average nose-cone half-angle, deg	2.6
Location of the forward end of the cylindrical-section	Station 23.37
Location of the cylindrical base	Station 35.17
Cylindrical-section diameter, in.	2.250
Base annulus area, sq ft	0.0058
Chamber area, sq ft	0.0218
Inclination of cylinder relative to wing reference plane, deg	2.00

TABLE II.- GEOMETRIC CHARACTERISTICS OF THE MODELS - Concluded

Engine pods used with six-pod configuration:	
Length, inlet spike tip to exit, in.	8.557
Length, inlet lip to exit, in.	6.732
Maximum diameter, in.	1.254
Capture area, per pod, sq ft	0.0056
Exit area, per pod, sq ft	0.0041
Base annulus area, per pod, sq ft	0.0036
Longitudinal location of inlet spike tip:	
Inboard pods	Station 28.62
Center pods	Station 35.07
Outboard pods	Station 40.42
Lateral location of inlet spike tip from the plane of symmetry, in.:	
Inboard pods	2.70
Center pods	5.24
Outboard pods	7.78
Distance of inlet spike tip below lower wing surface, in.:	
Inboard pods	1.28
Center pods	1.28
Outboard pods	1.28
Inclination of the pod center line relative to the wing reference plane, nose upward, deg:	
Inboard pods	3.25
Center pods	0.92
Outboard pods	-0.33
Toe-in angle of the pod center line, deg:	
Inboard pods	0.66
Center pods	2.66
Outboard pods	4.21
Pod support strut:	
Sweepback of leading and trailing edges relative to the local wing surface, deg	60
Chord parallel to the local wing surface, in.	4.00
Airfoil section parallel to the local wing surface	3-percent-thick circular arc
Clustered engine inlet-duct assembly:	
Location of base	Station 34.22
Length of assembly, in.	19.27
Maximum height of assembly, in.	2.588
Maximum width of assembly, in.	3.934
Capture area, total for both sides, sq ft	0.0288
Exit area, total for four exits, sq ft	0.0208
Base area, sq ft	0.0168
Chamber area, sq ft	0.0192
Inlet-ramp wedge angle, deg	6.00
Sweepback angle of upper and lower inlet lips, deg	65.65
Angle of the forward part of the duct outer side wall relative to the plane of symmetry, deg	5.48
Boundary-layer-diverter wedge angle, deg	9.44

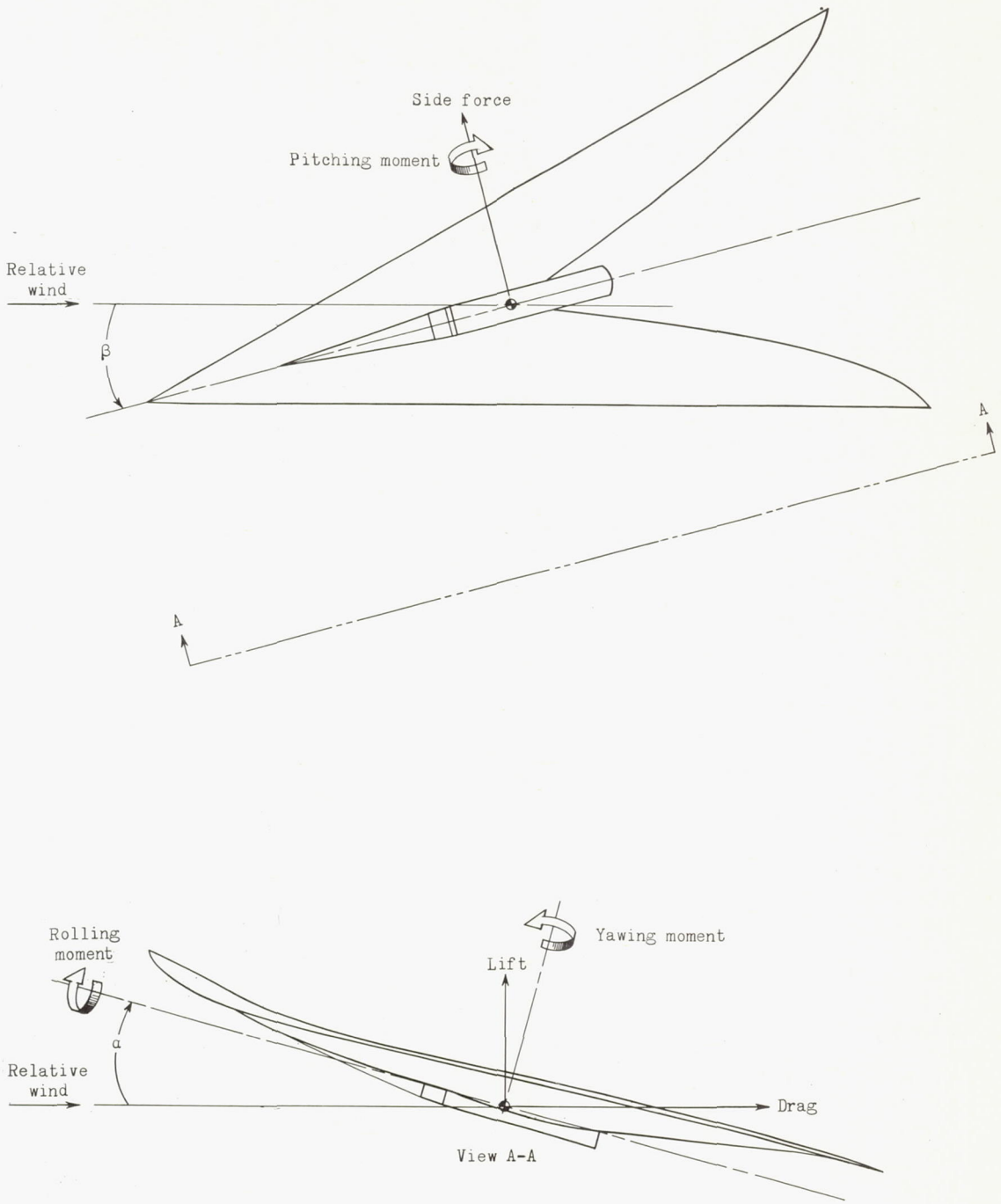

Figure 1.- Axes used for data presentation.

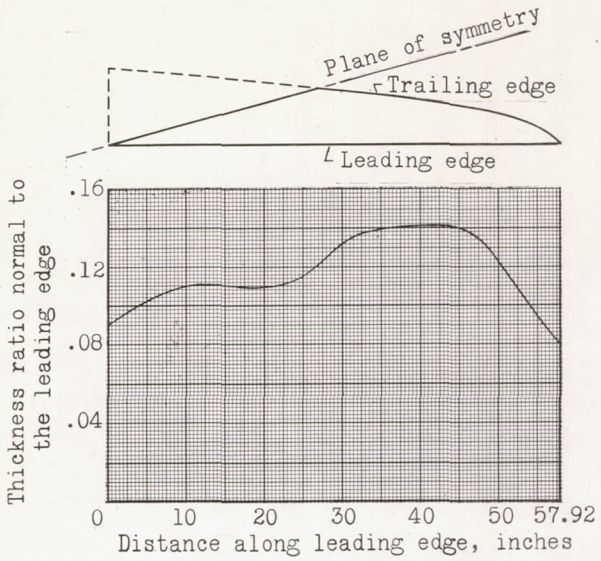

(a) Thickness distribution.

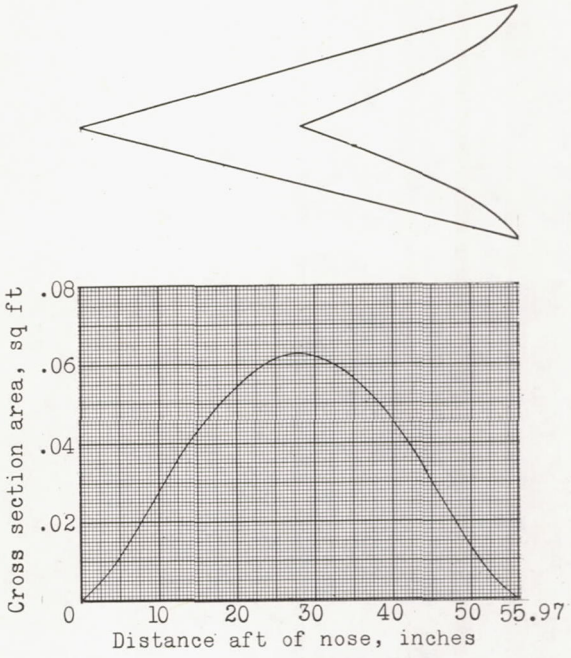

(b) Cross-section area distribution (sections normal to the longitudinal axis).

Figure 2.- Wing thickness.

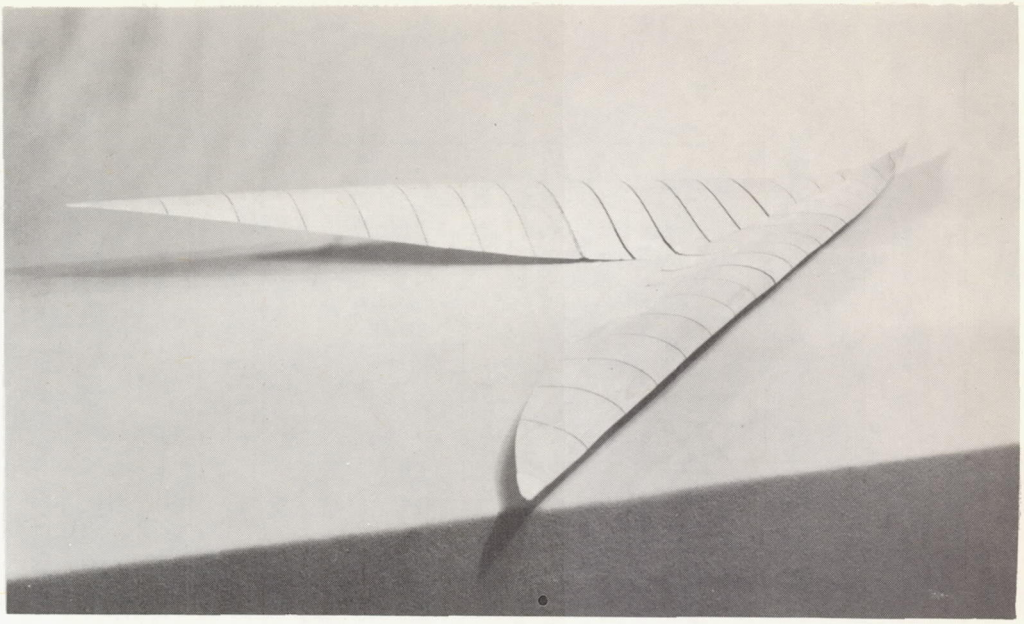

L-58-502

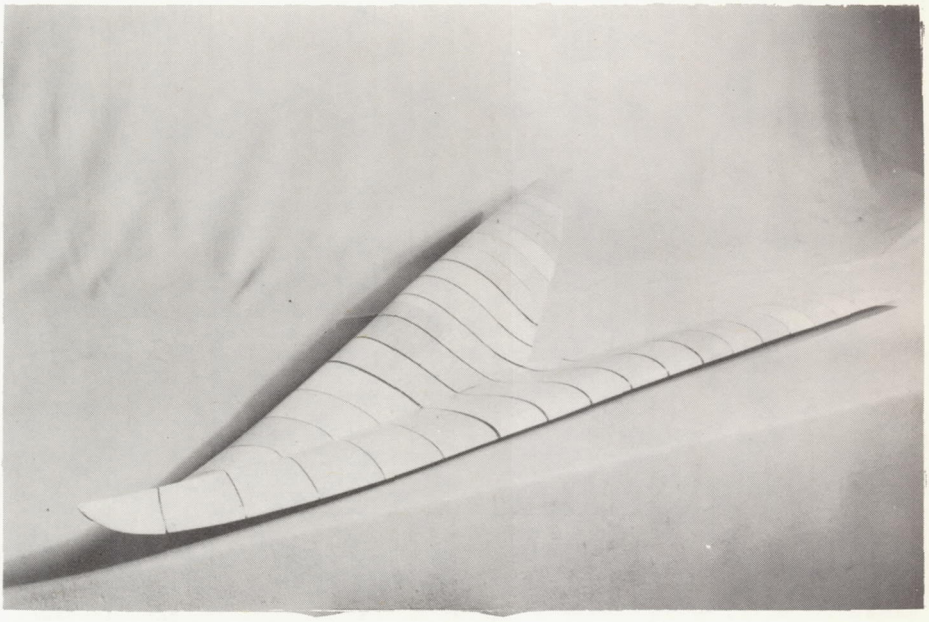

L-58-503

Figure 3.- Photographs of a wood mock-up of the wing showing upper-surface contours. Sections indicated are normal to the leading edge.

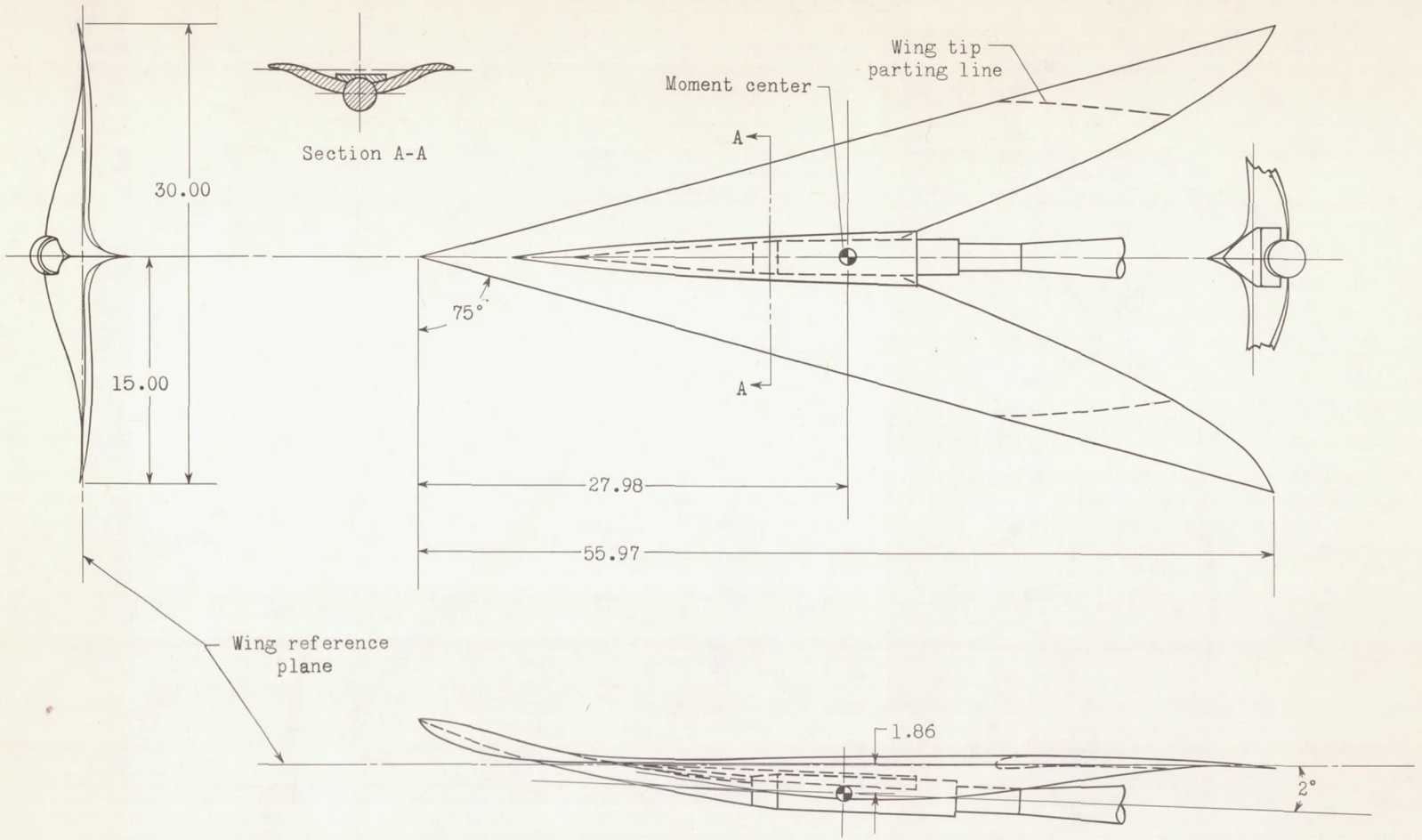

(a) Wing alone with rectangular body fairing on upper surface. The basic test configuration was the same but with the rectangular fairing removed (circular body fairing only used).

Figure 4.- Three-view drawings of the test configurations.

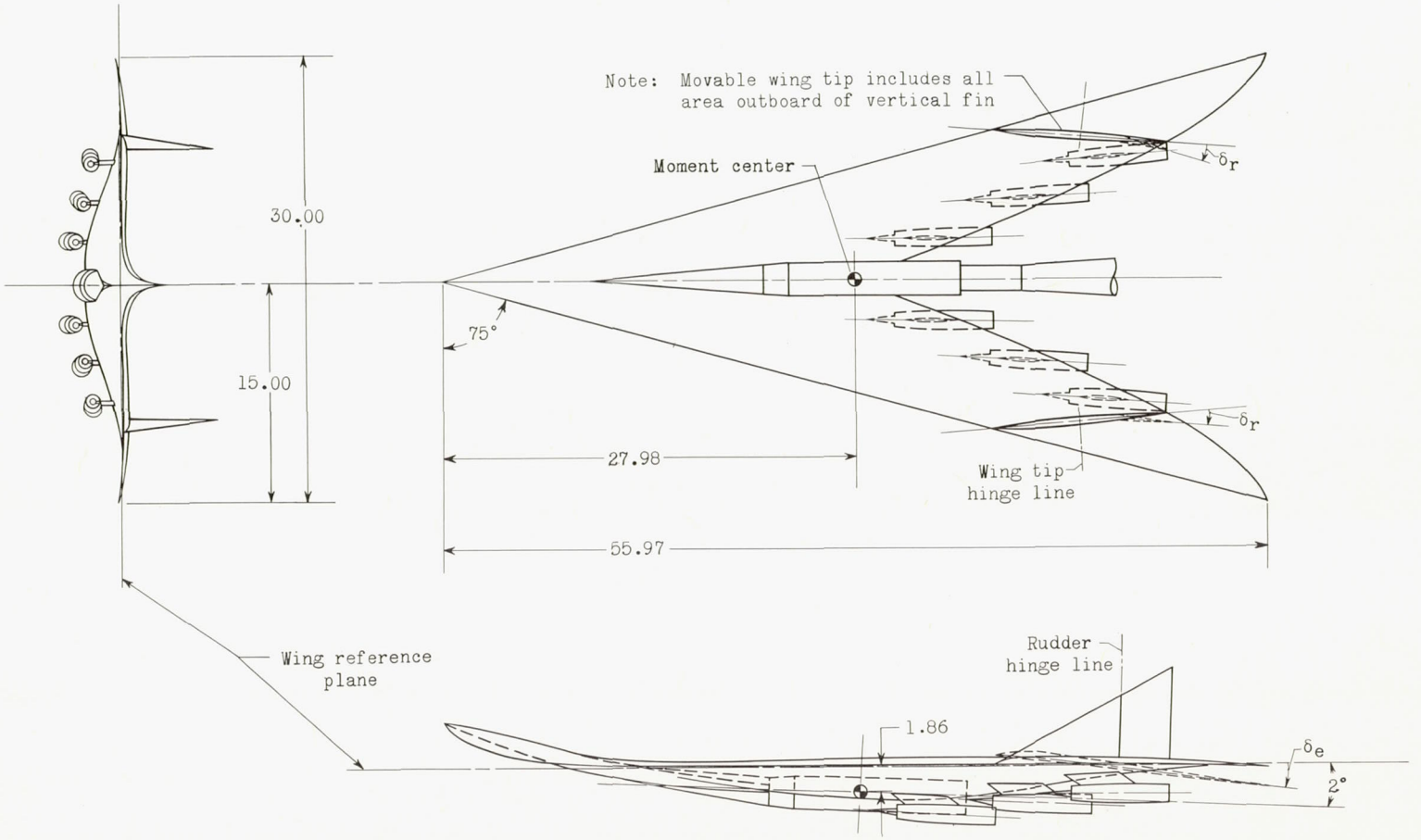

(b) Complete-airplane configuration with six underslung pods and upper-surface fins.

Figure 4.- Continued.

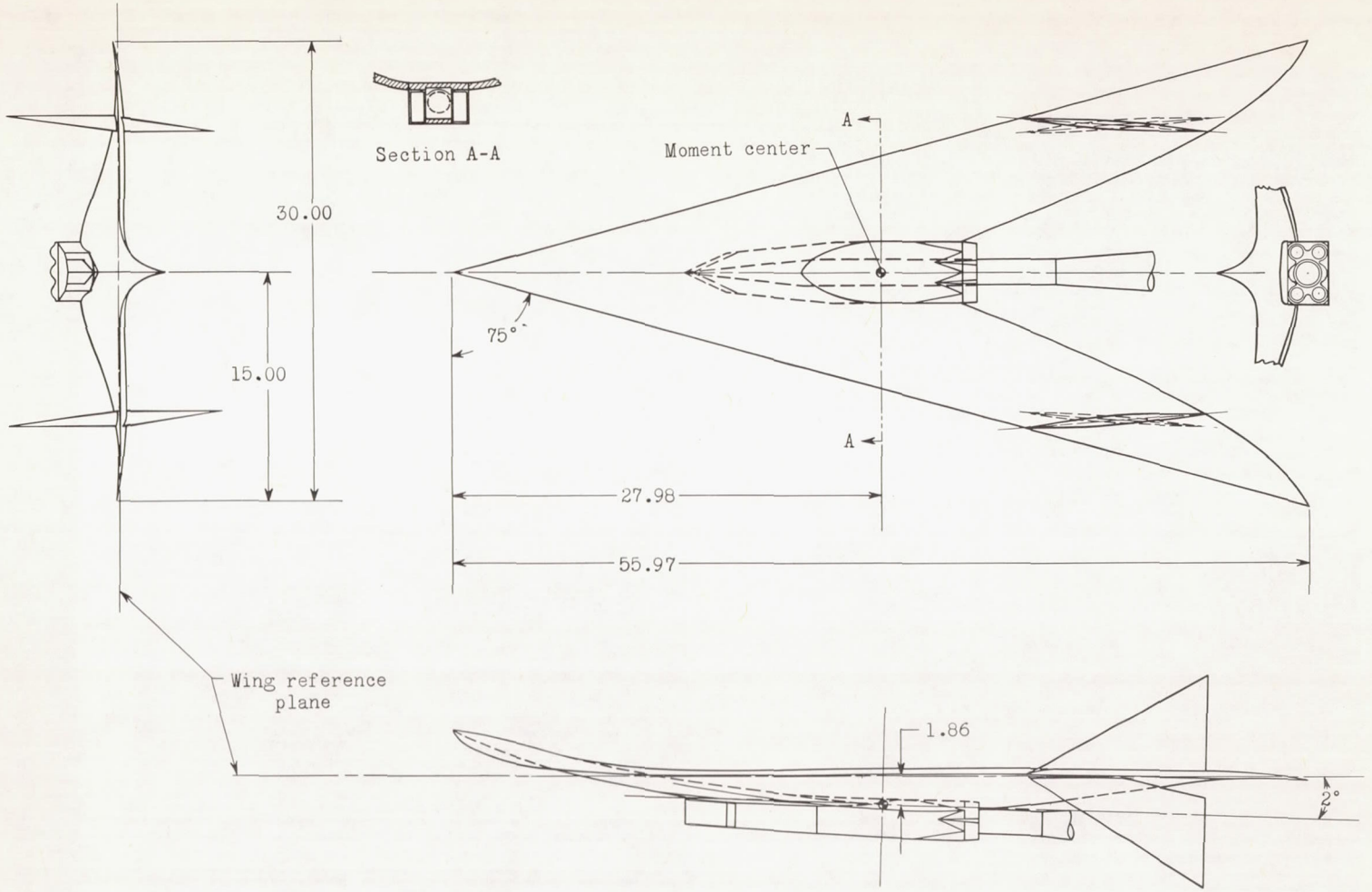

(c) Complete-airplane configuration with clustered engine installation and upper- and lower-surface fins.

Figure 4.- Concluded.

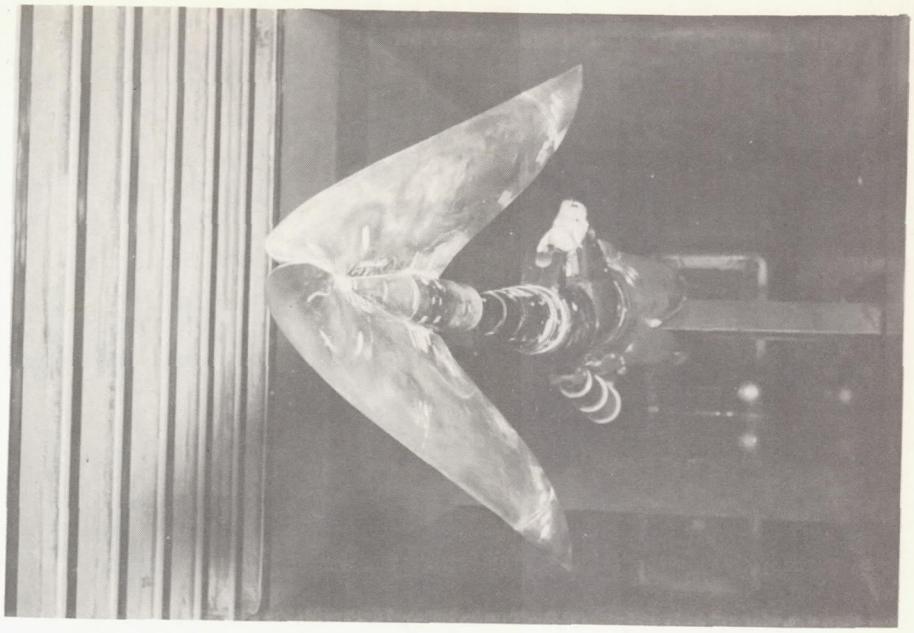

(a) Wing alone. L-57-5560

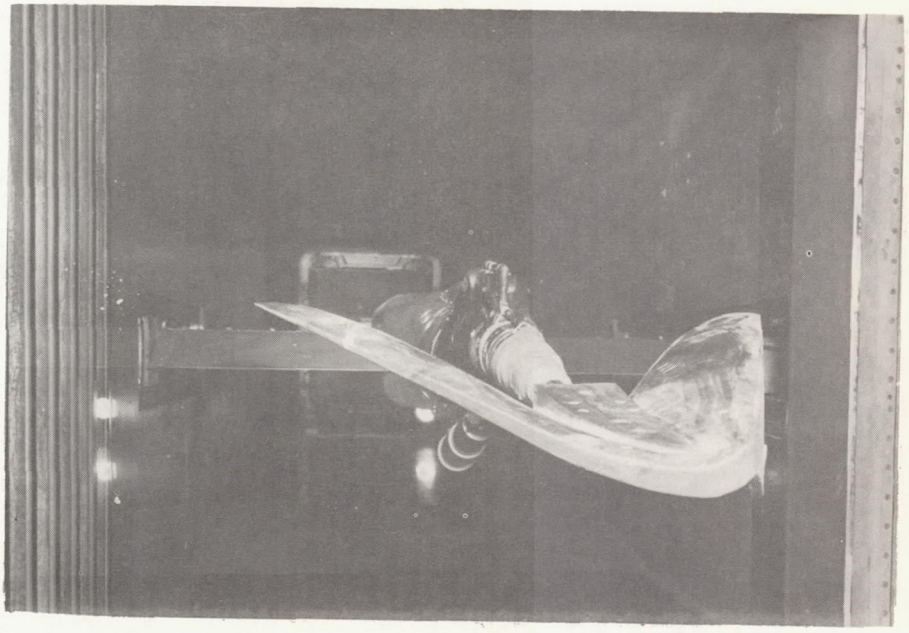

(b) Wing alone with rectangular body fairing. L-58-300

Figure 5.- Photographs of several model configurations.

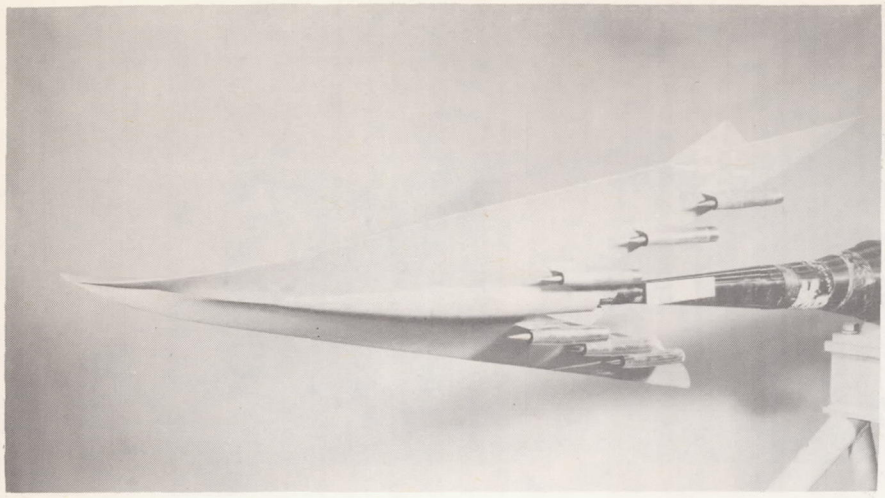

L-58-826

(c) Complete airplane configuration with underslung pods and upper-surface fins.

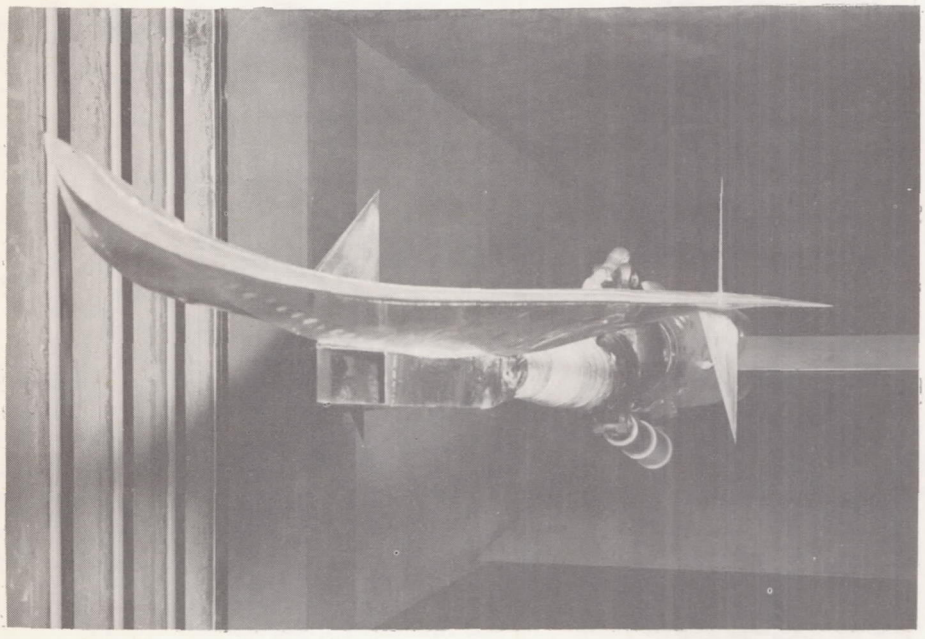

L-57-5614

(d) Complete airplane configuration with clustered engine installation. Both upper- and lower-surface fins are skewed so as to be aligned with local air flow at design lifting conditions.

Figure 5.- Concluded.

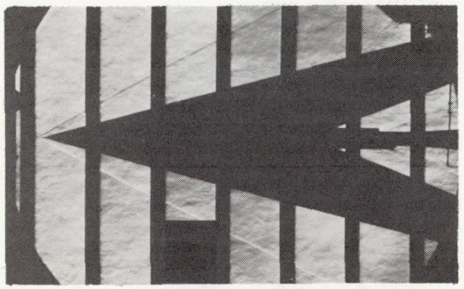

M=2.36; α=2°

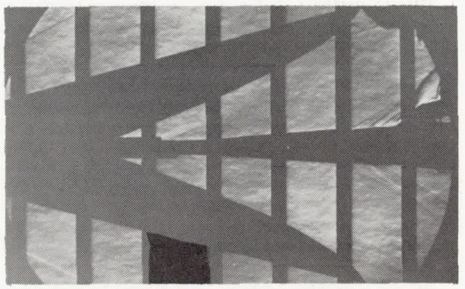

M=2.36; α=2°

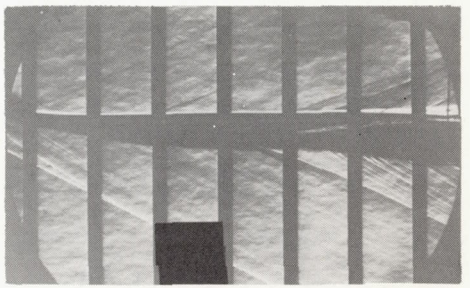

M=2.36; α=2.5°

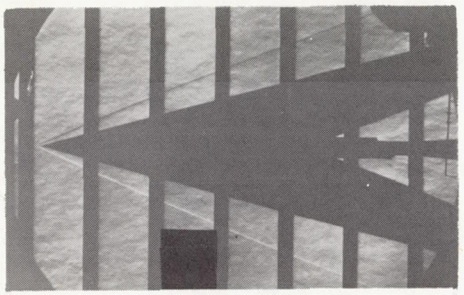

M=2.87; α=2°

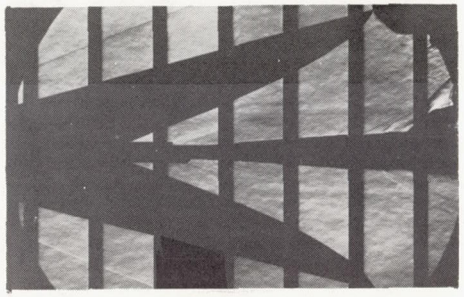

M=2.87; α=2°

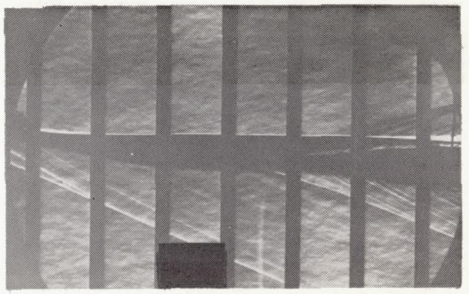

M=2.87; α=2.2°

(a) Wing alone. L-58-1673

Figure 6.- Schlieren photographs of the model.

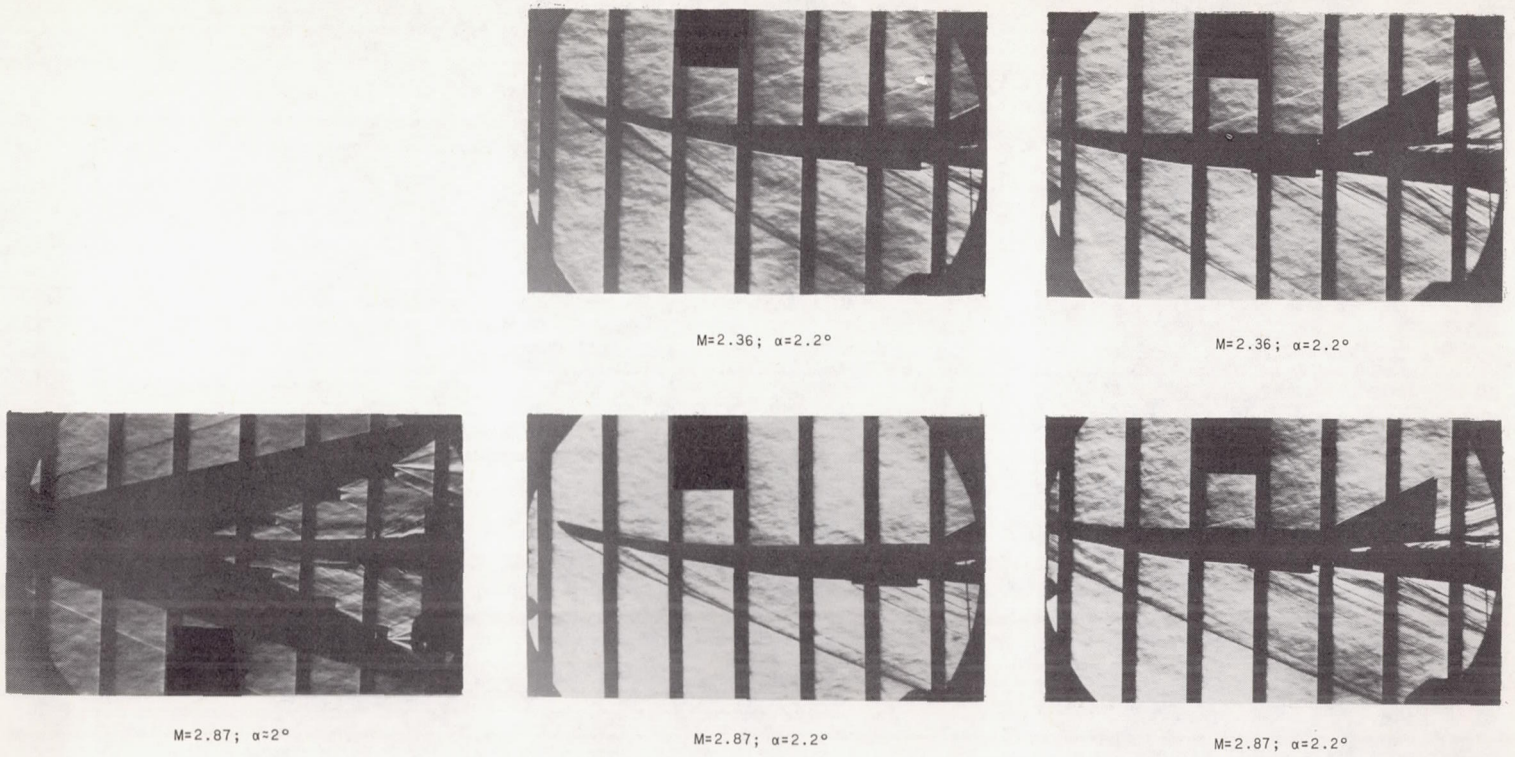

(b) Complete model with six underslung pods and upper-surface fins. $\delta_e = 0^\circ$. L-58-1674

Figure 6.- Continued.

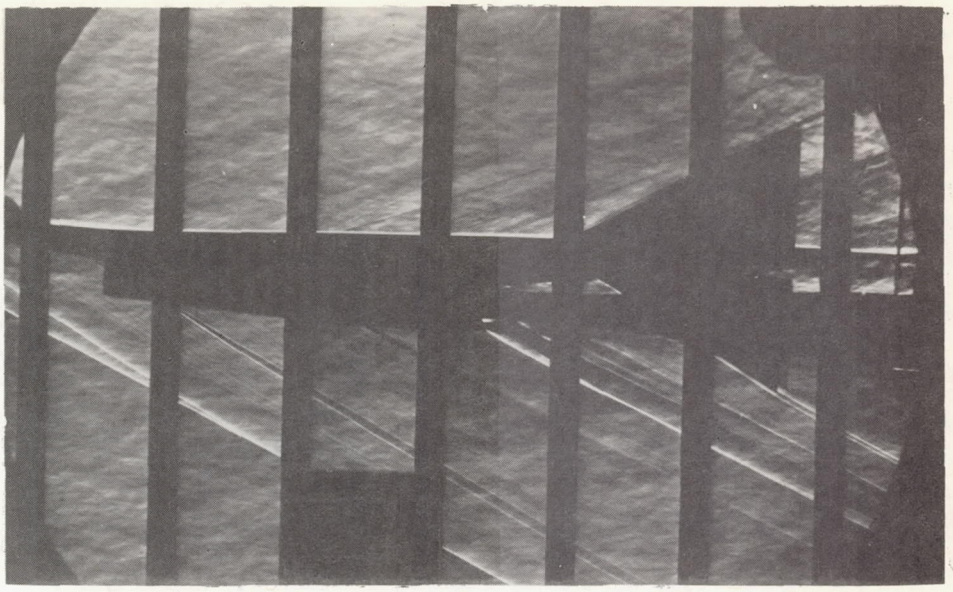

M=2.36; α=2.5°

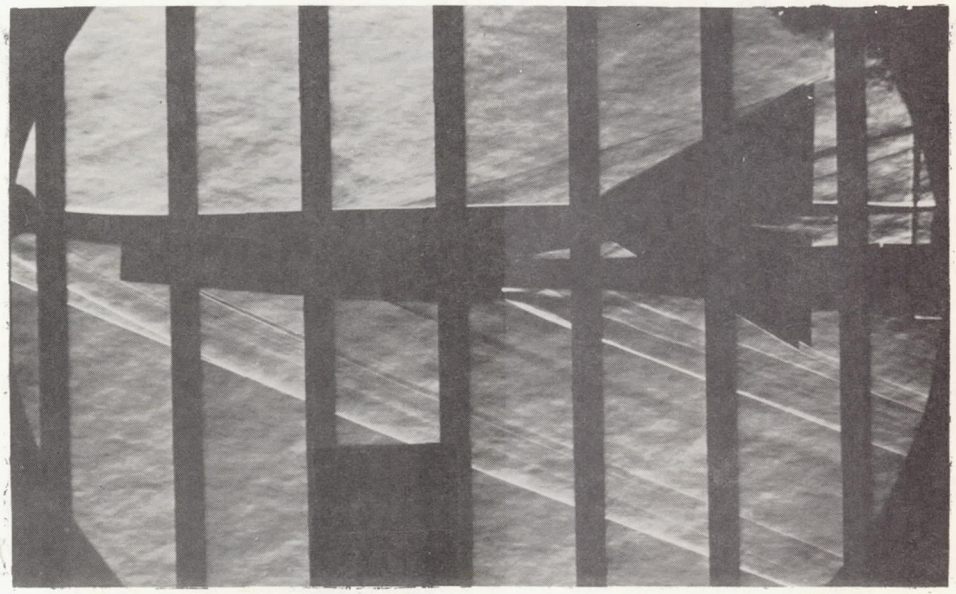

M=2.87; α=2.2°

L-58-1675

(c) Complete model with clustered engine installation. Both upper- and lower-surface fins. $\delta_e = 0^\circ$.

Figure 6.- Concluded.

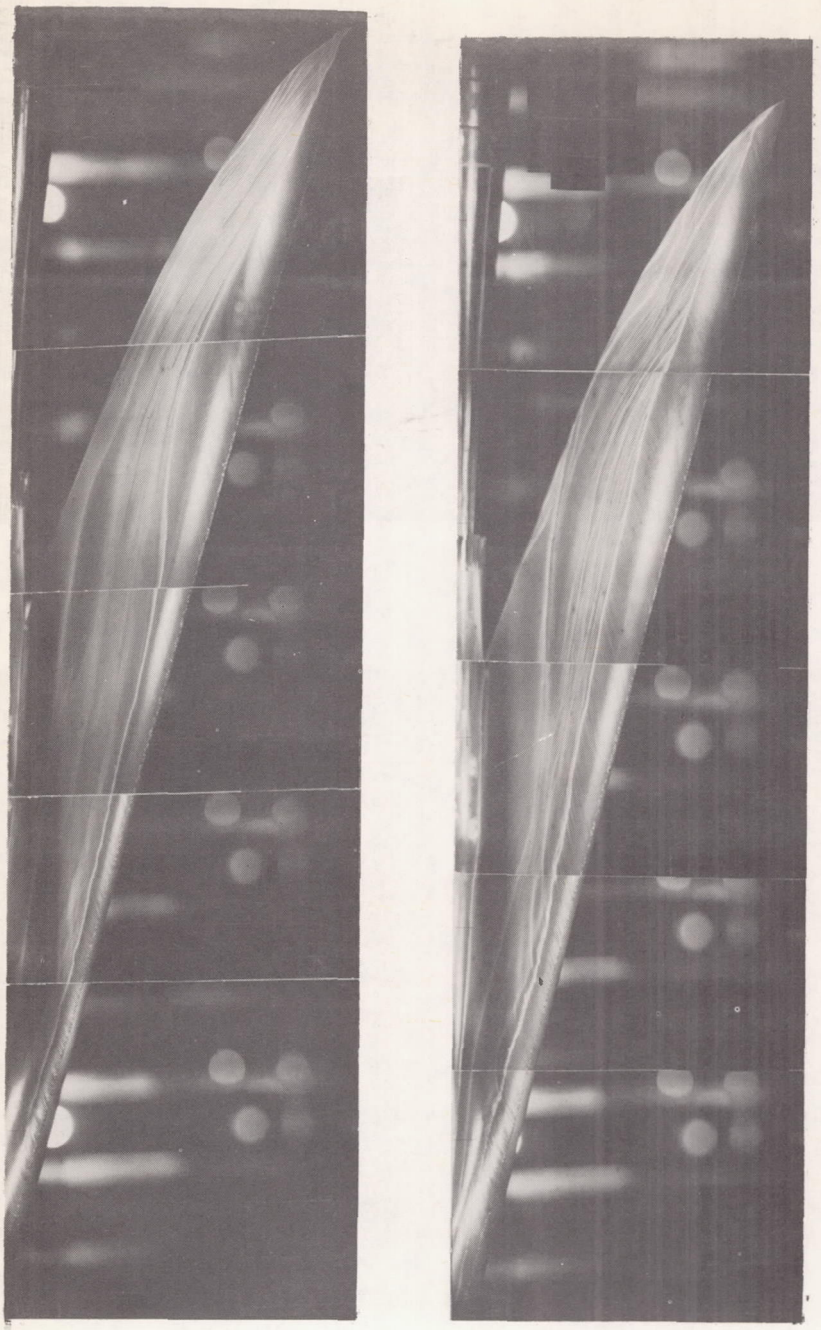

M = 2.36 M = 2.87

L-58-1676

Figure 7.- Oil-film-flow photographs of the wing alone. Fixed transition, $C_L \approx 0.1$; $R \approx 4.2 \times 10^6$.

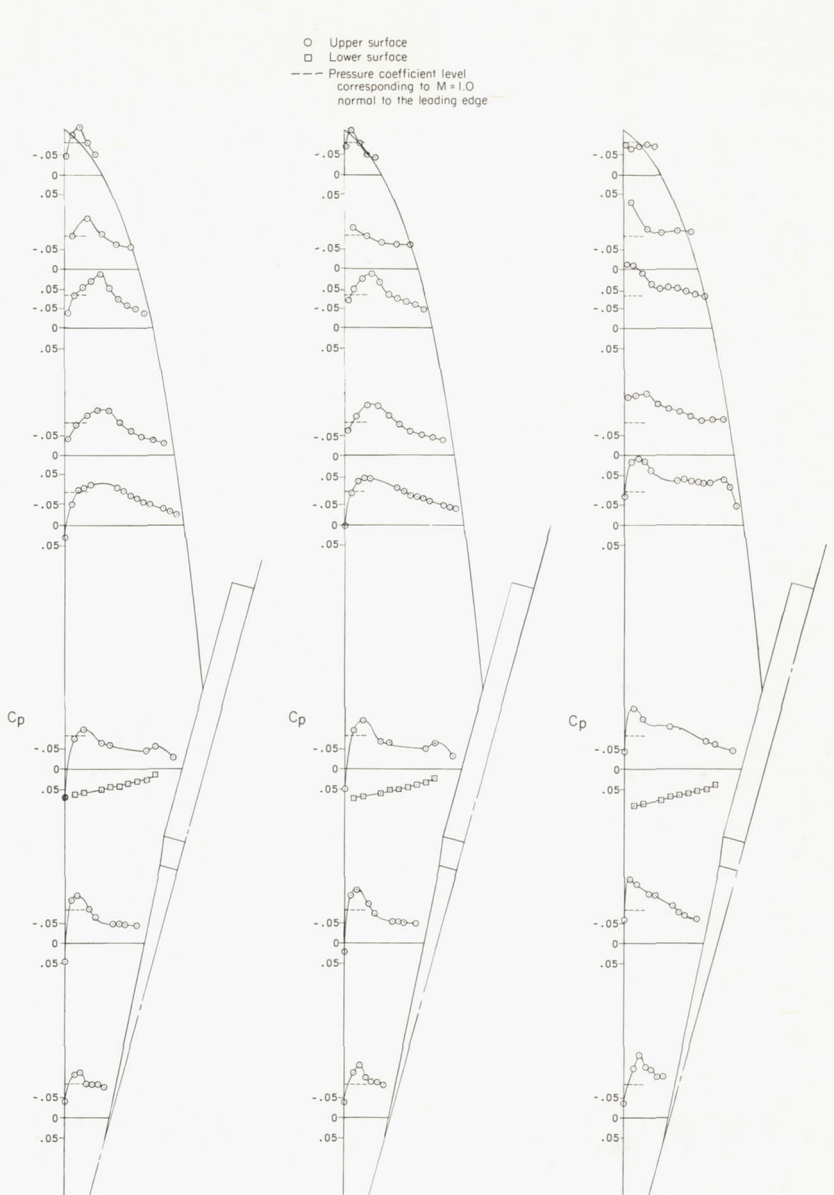

(a) M = 2.36.

Figure 8.- Pressure distribution on wing alone at angles of attack near design condition.

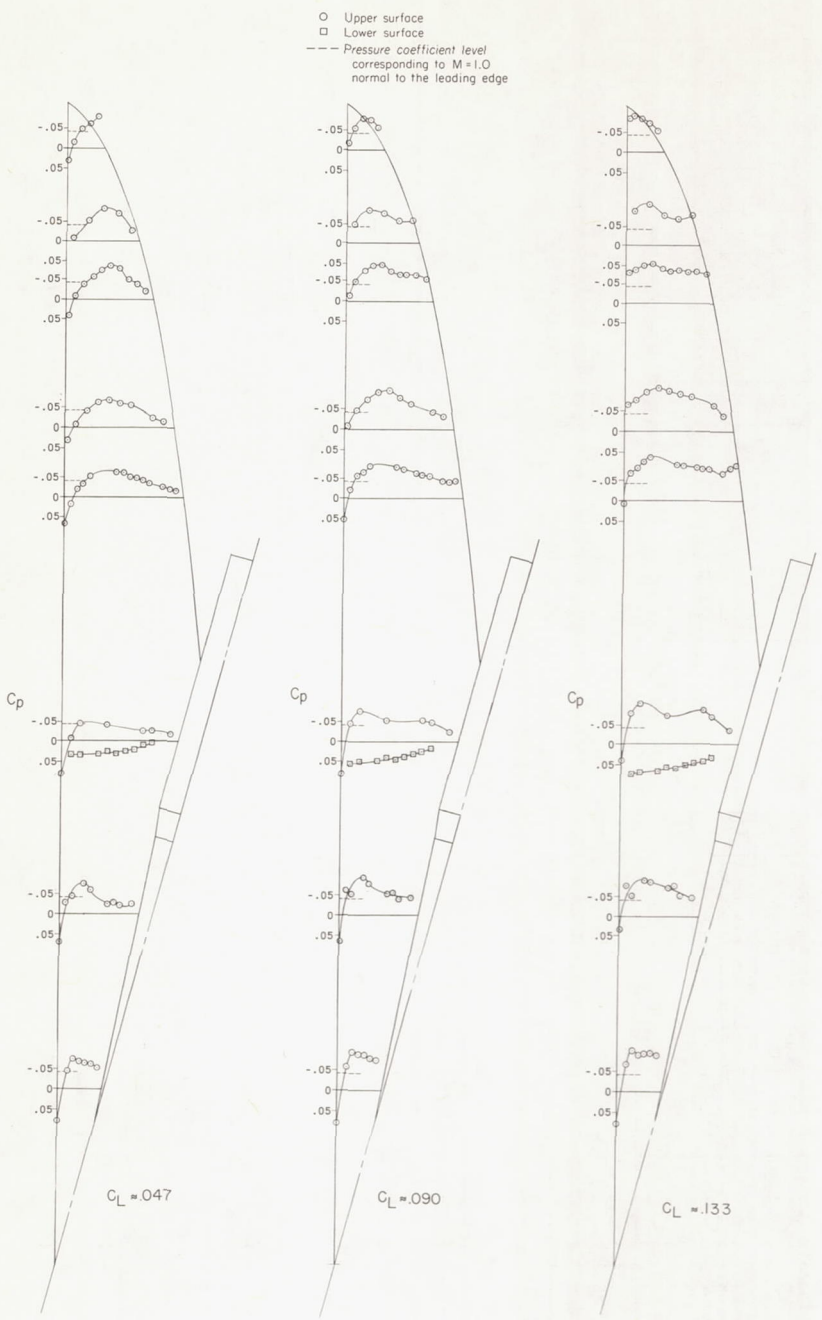

(b) M = 2.87.

Figure 8.- Concluded.

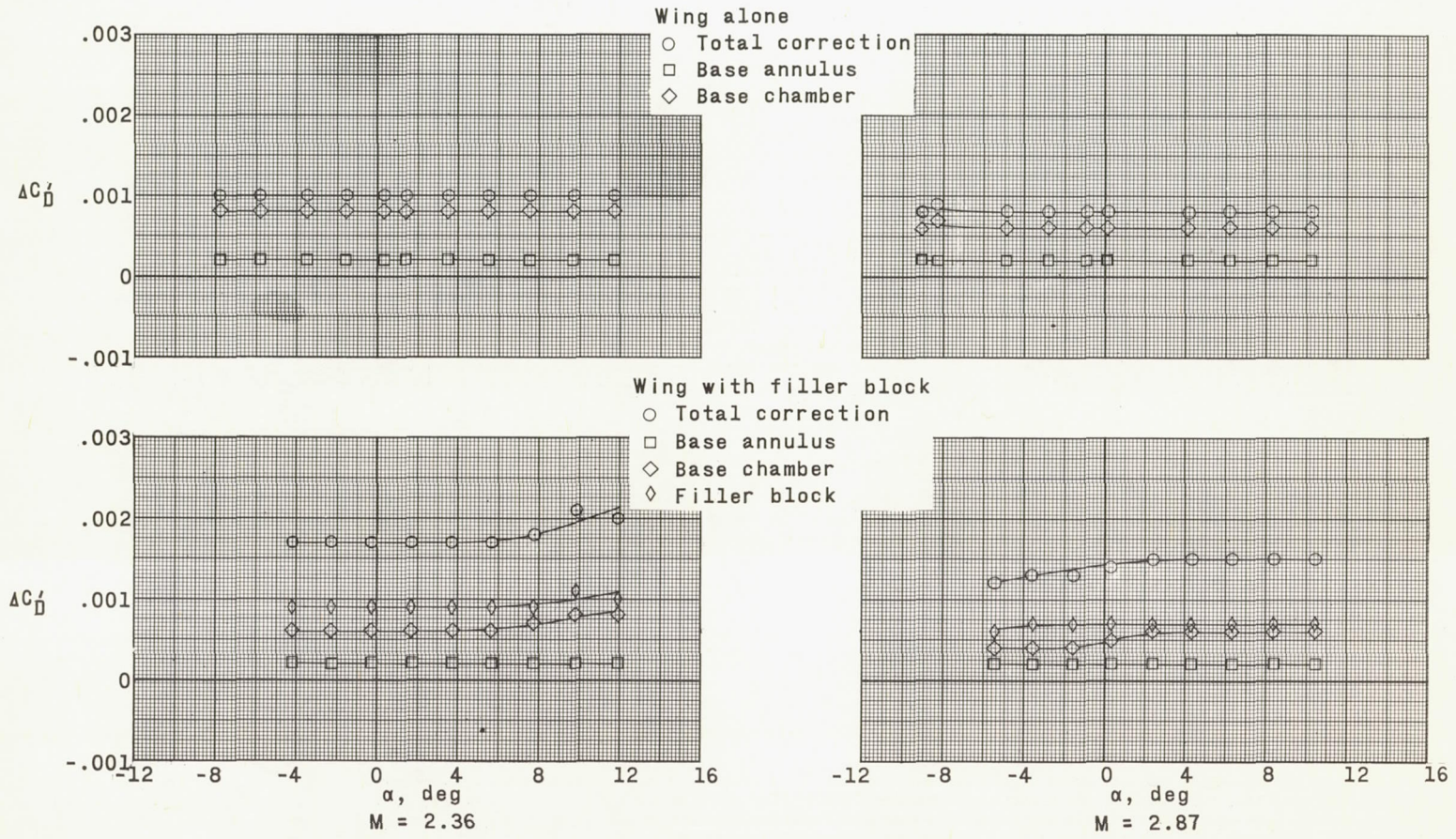

Figure 9.- Variation of base, chamber, and internal drag coefficients with angle of attack for various model configurations.

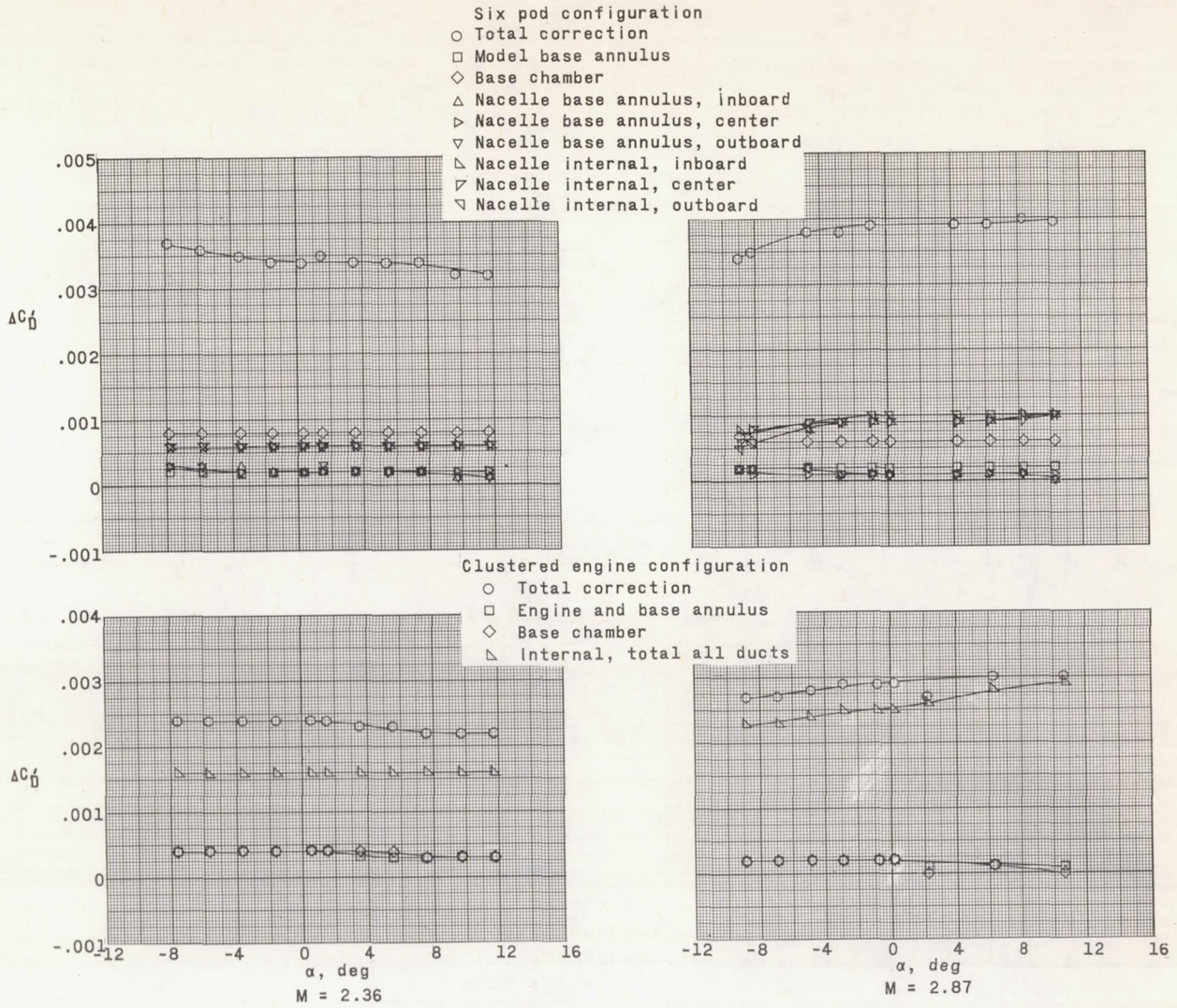

Figure 9.- Concluded.

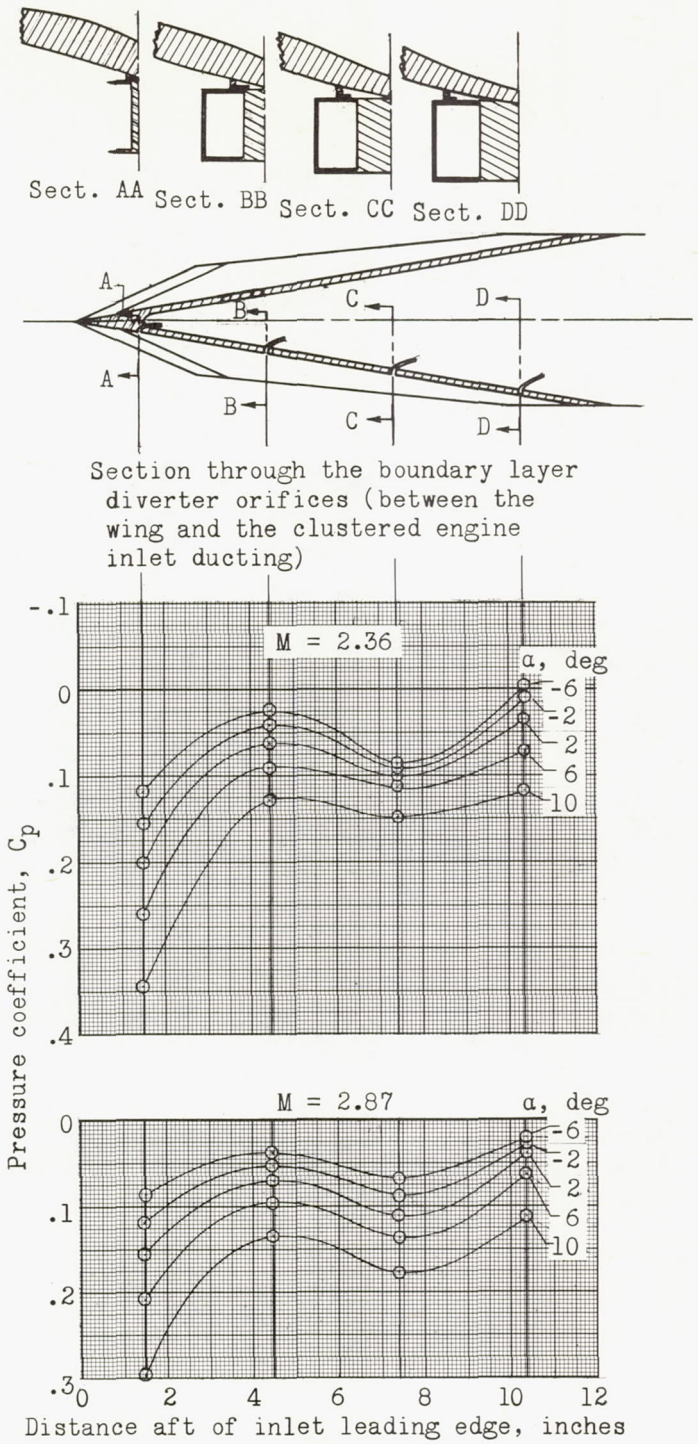

Figure 10.- Boundary-layer-diverter pressures for clustered engine configuration.

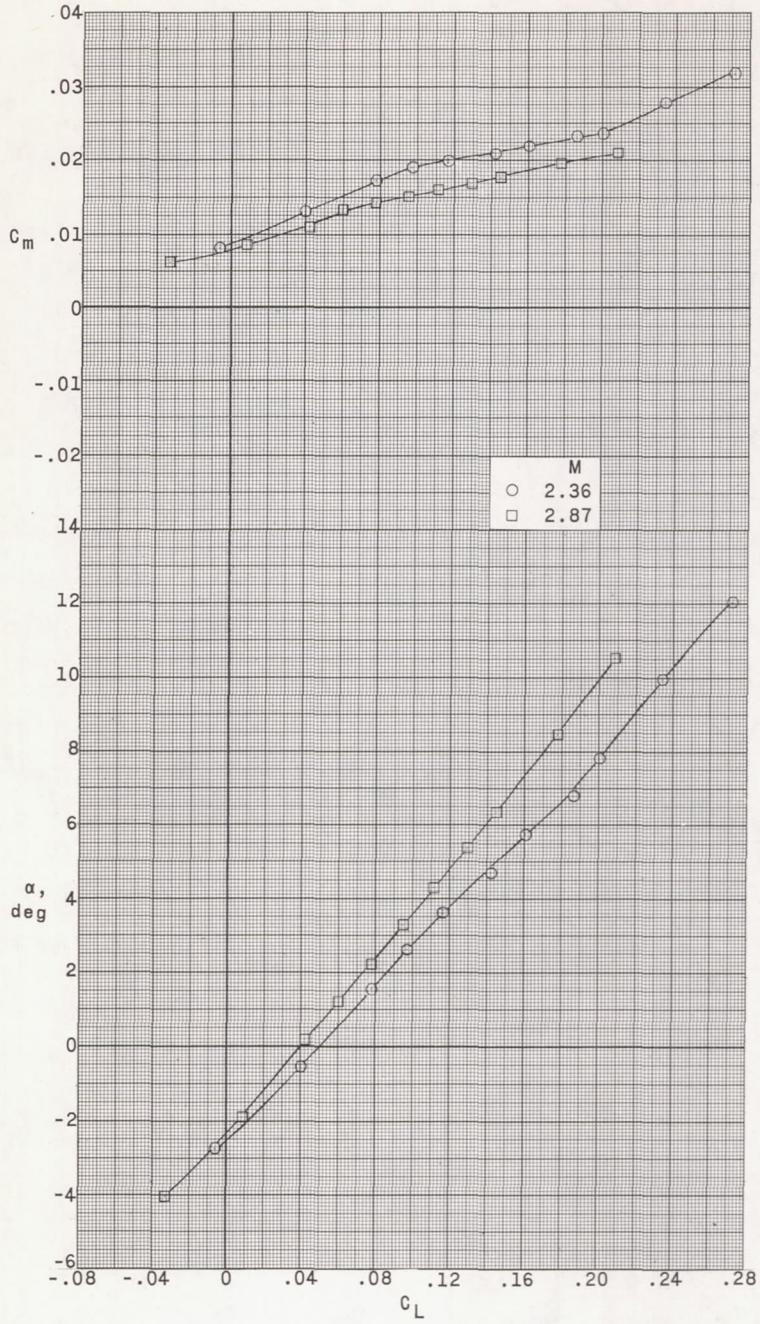

(a) Wing with tips removed.

Figure 11.- Longitudinal characteristics of the various model configurations.

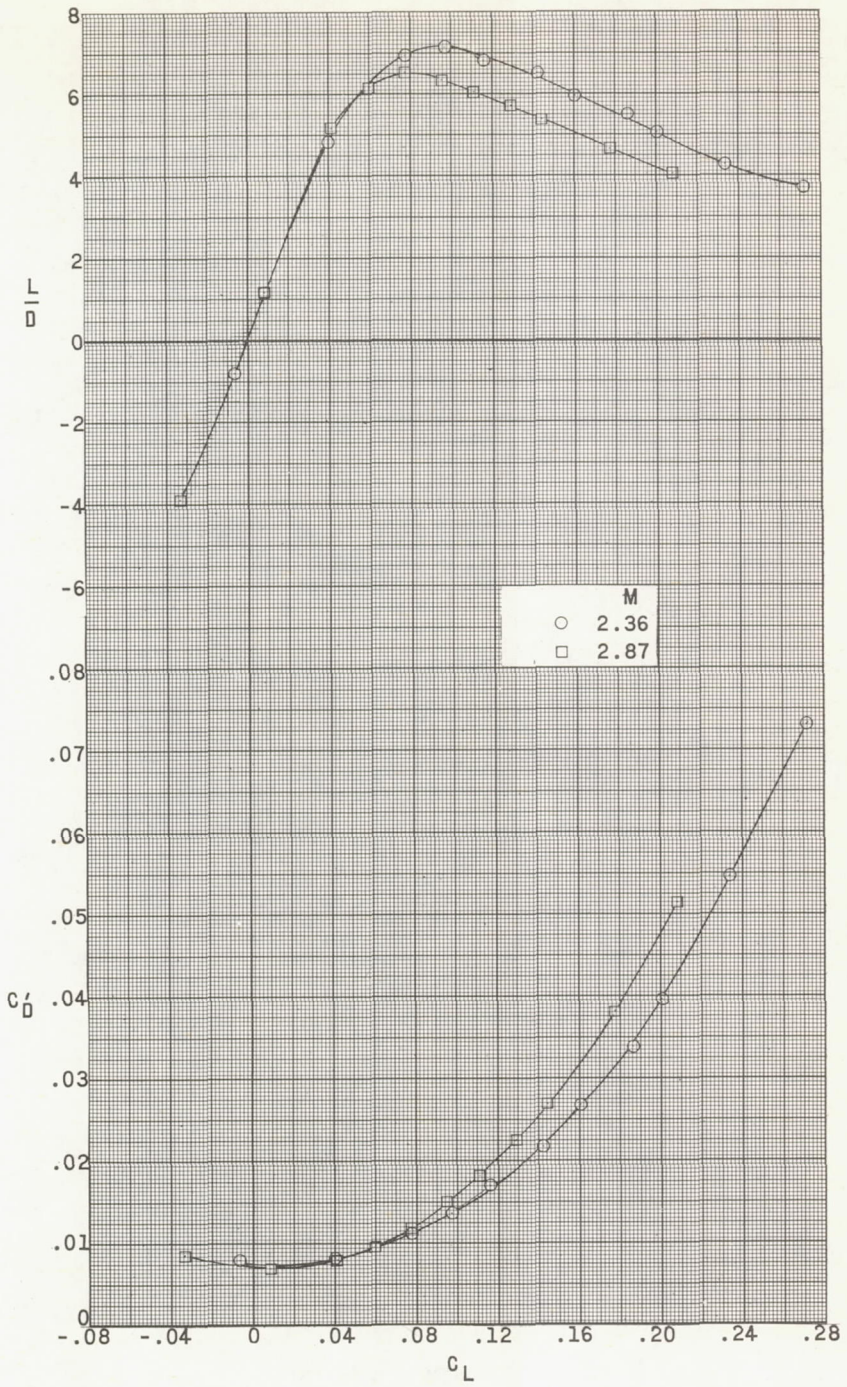

(a) Concluded.

Figure 11.- Continued.

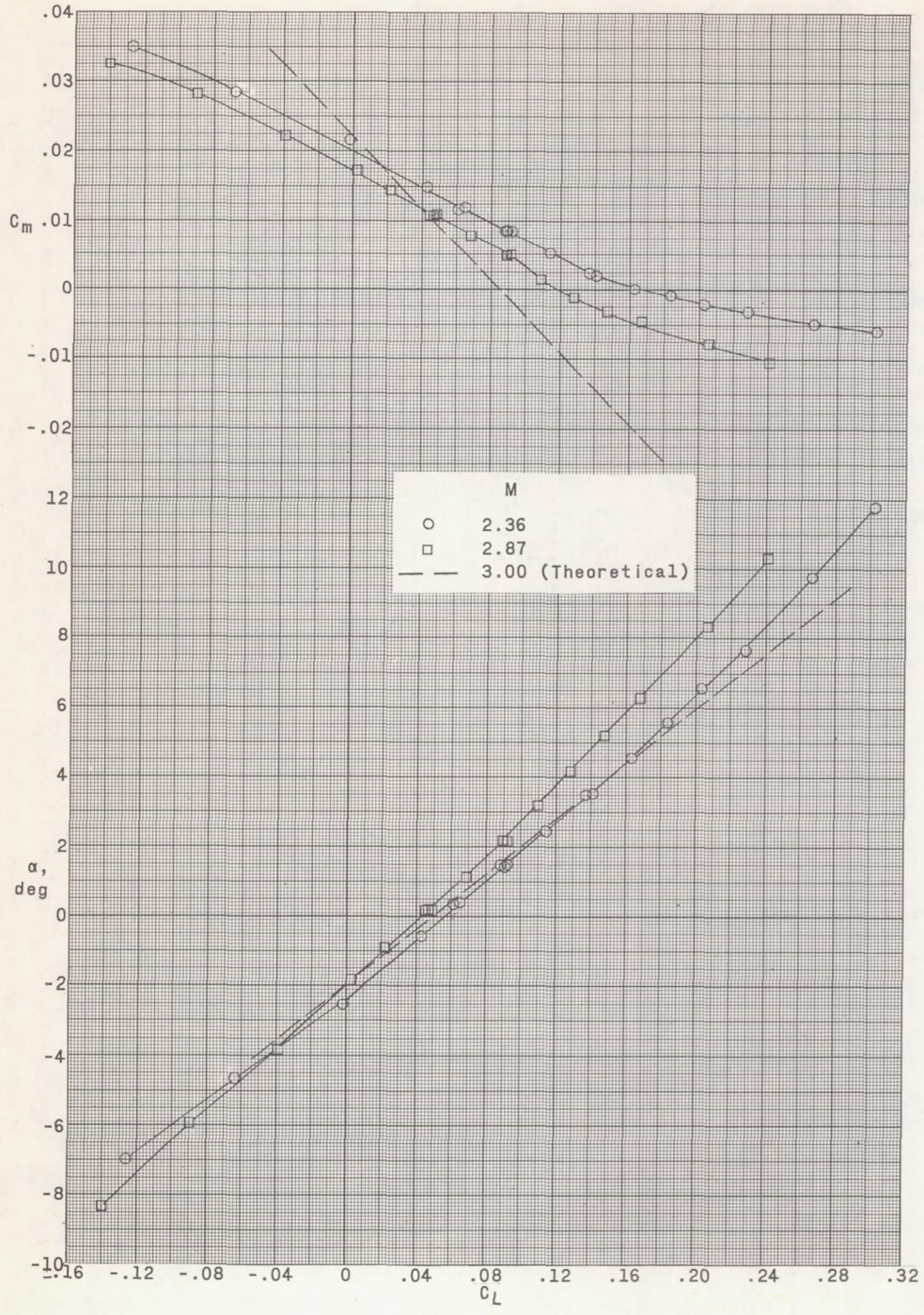

(b) Wing alone.

Figure 11.- Continued.

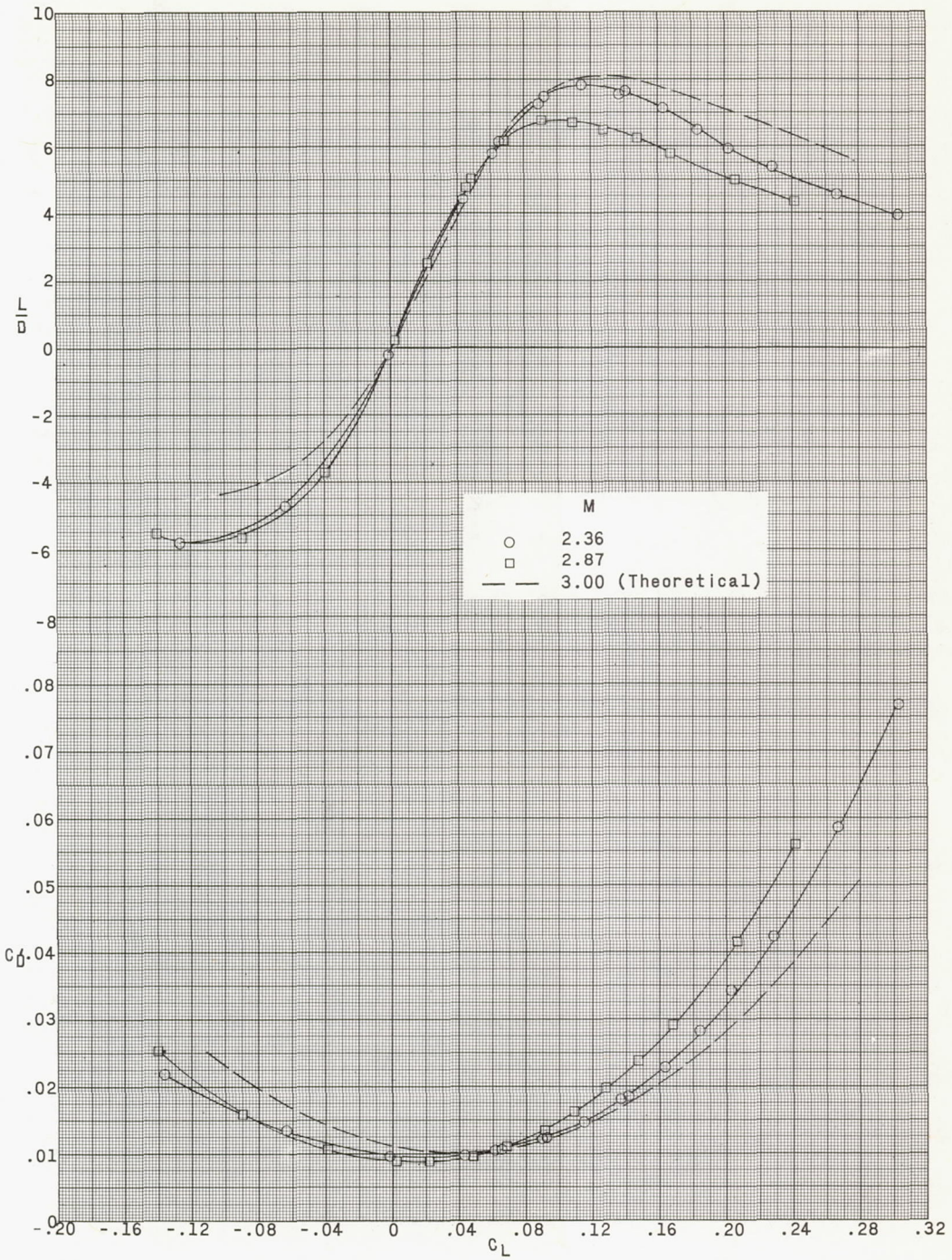

(b) Concluded.

Figure 11.- Continued.

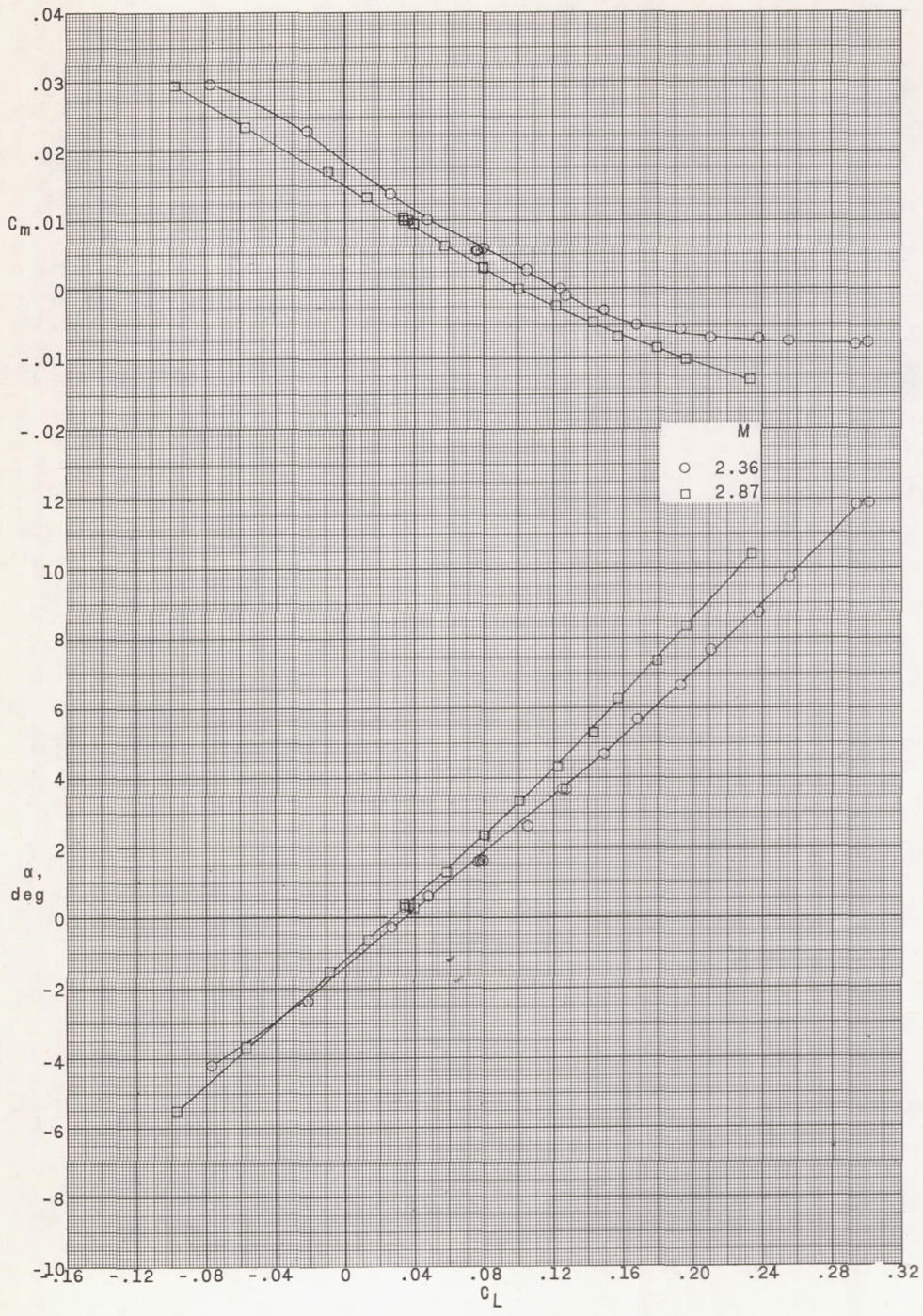

(c) Wing with rectangular body fairing.

Figure 11.- Continued.

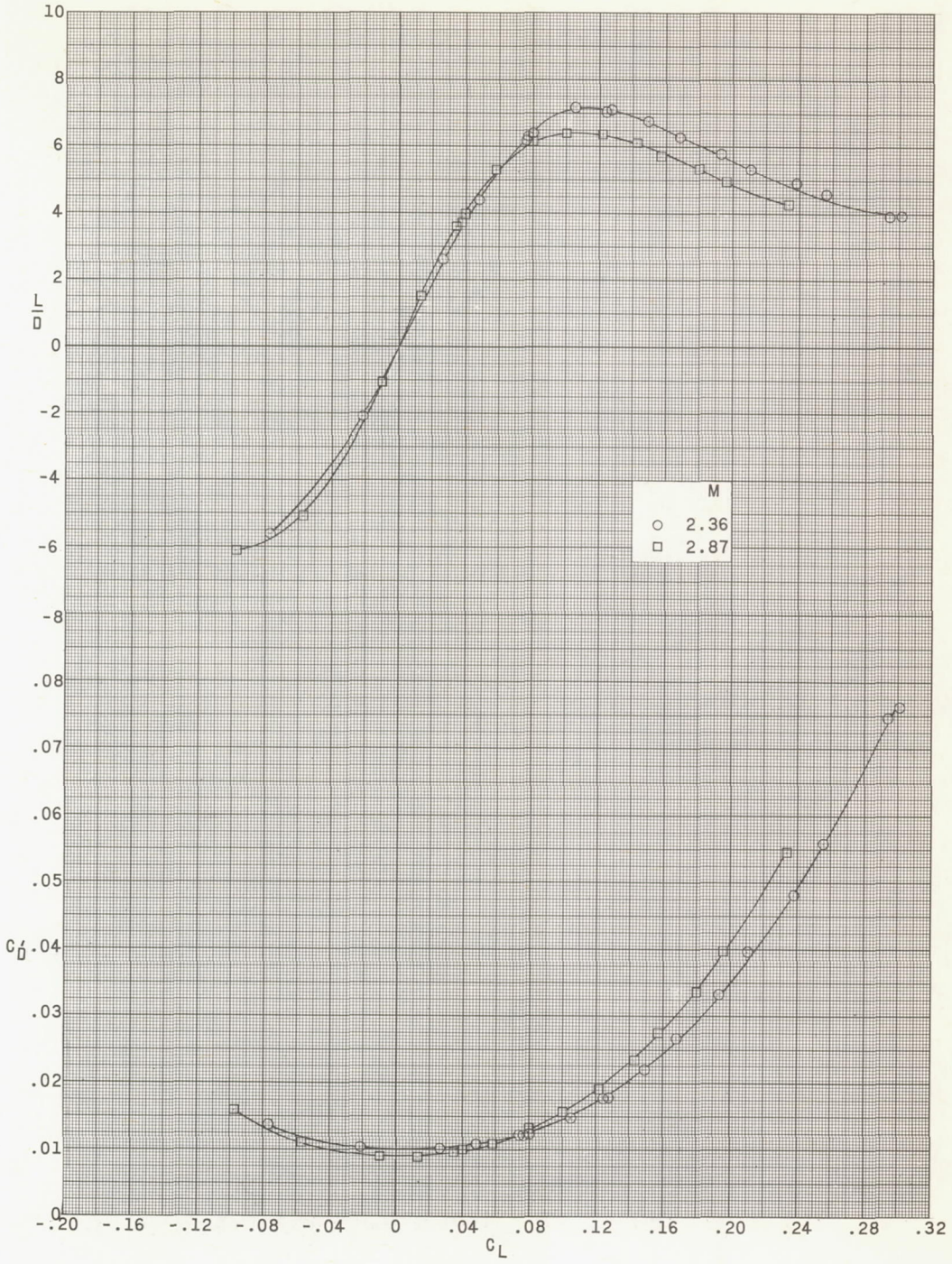

(c) Concluded.

Figure 11.- Continued.

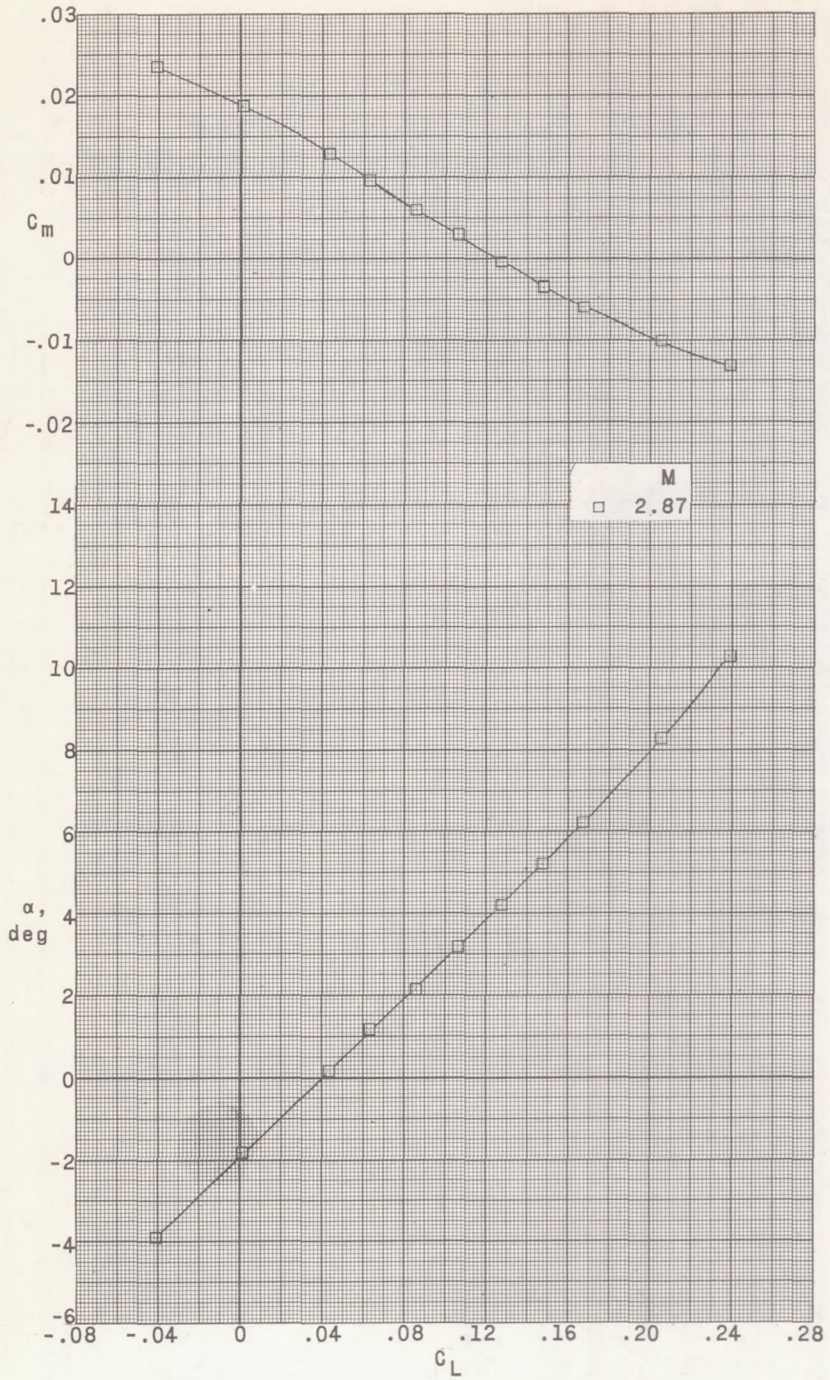

(d) Wing with upper-surface fins. $\delta_r = 0^\circ$.

Figure 11.- Continued.

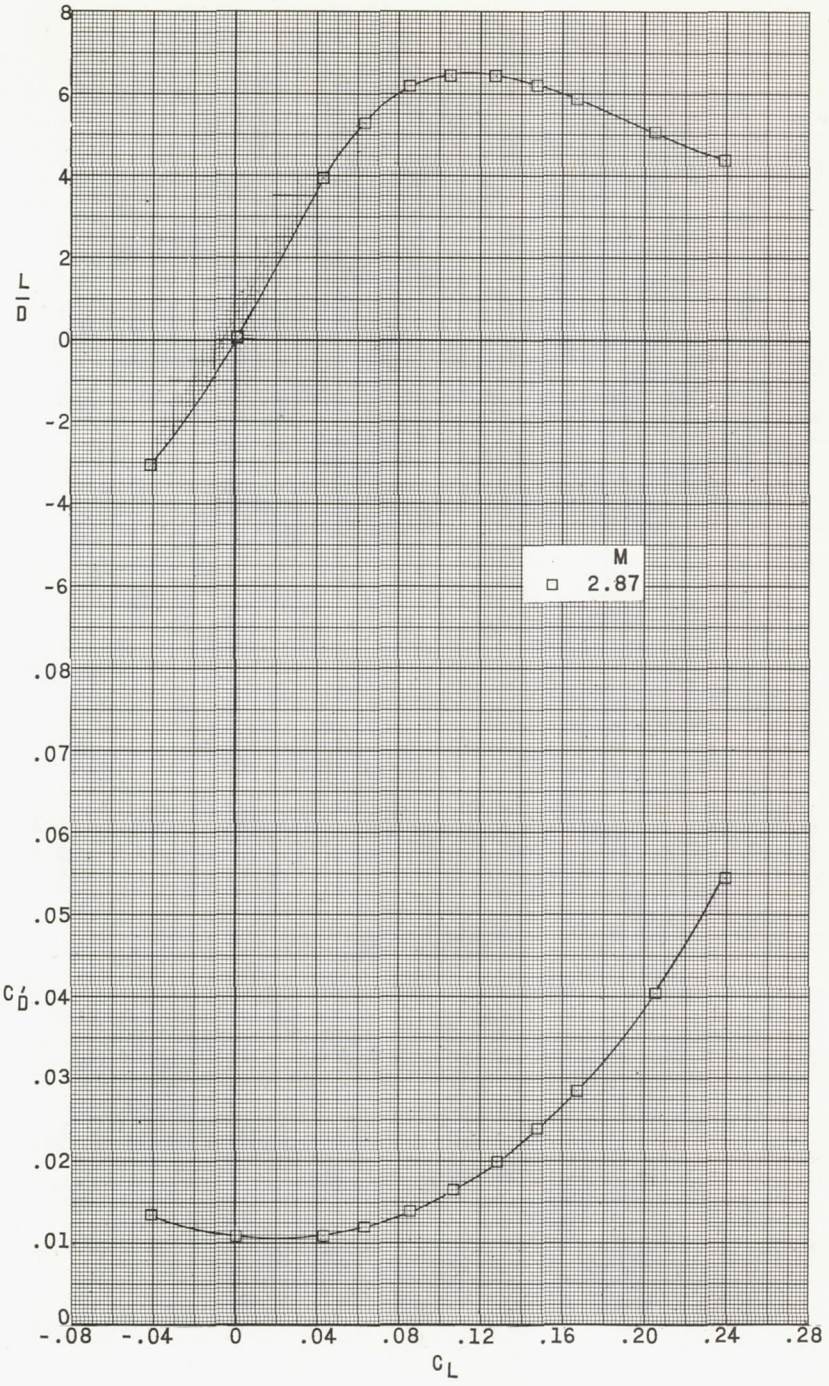

(d) Concluded.

Figure 11.- Continued.

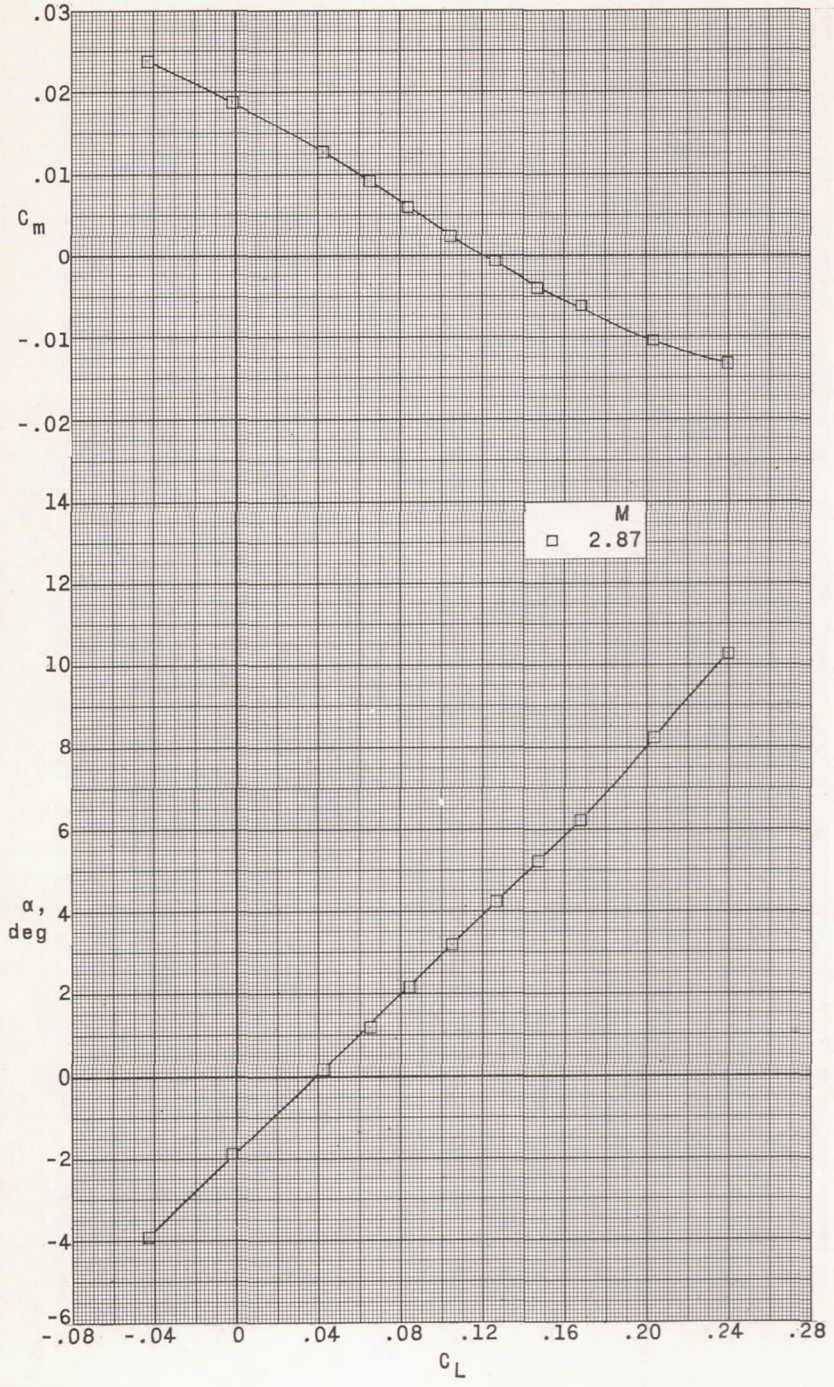

(e) Wing with upper-surface fins deflected. $\delta_r = 5^\circ$.

Figure 11.- Continued.

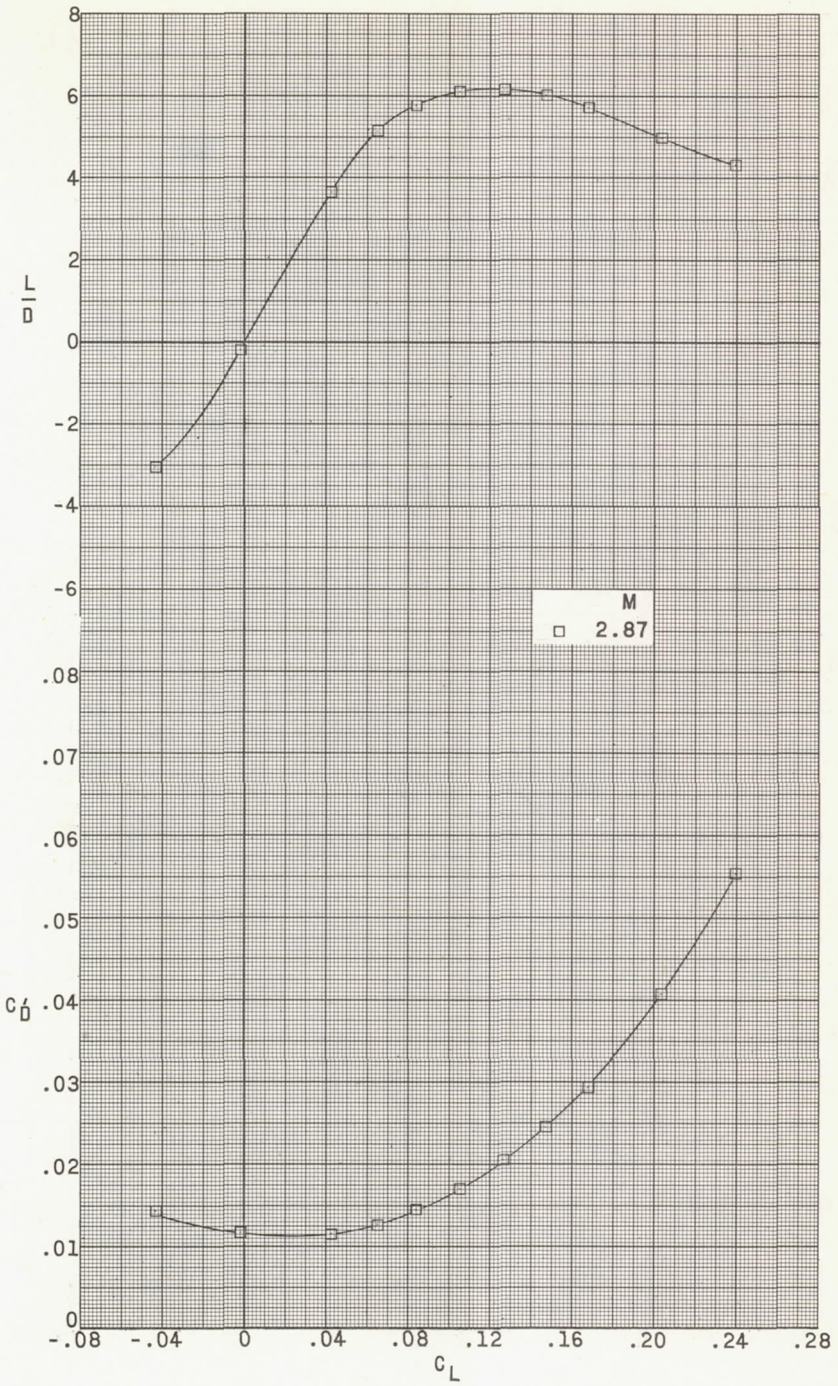

(e) Concluded.

Figure 11.- Continued.

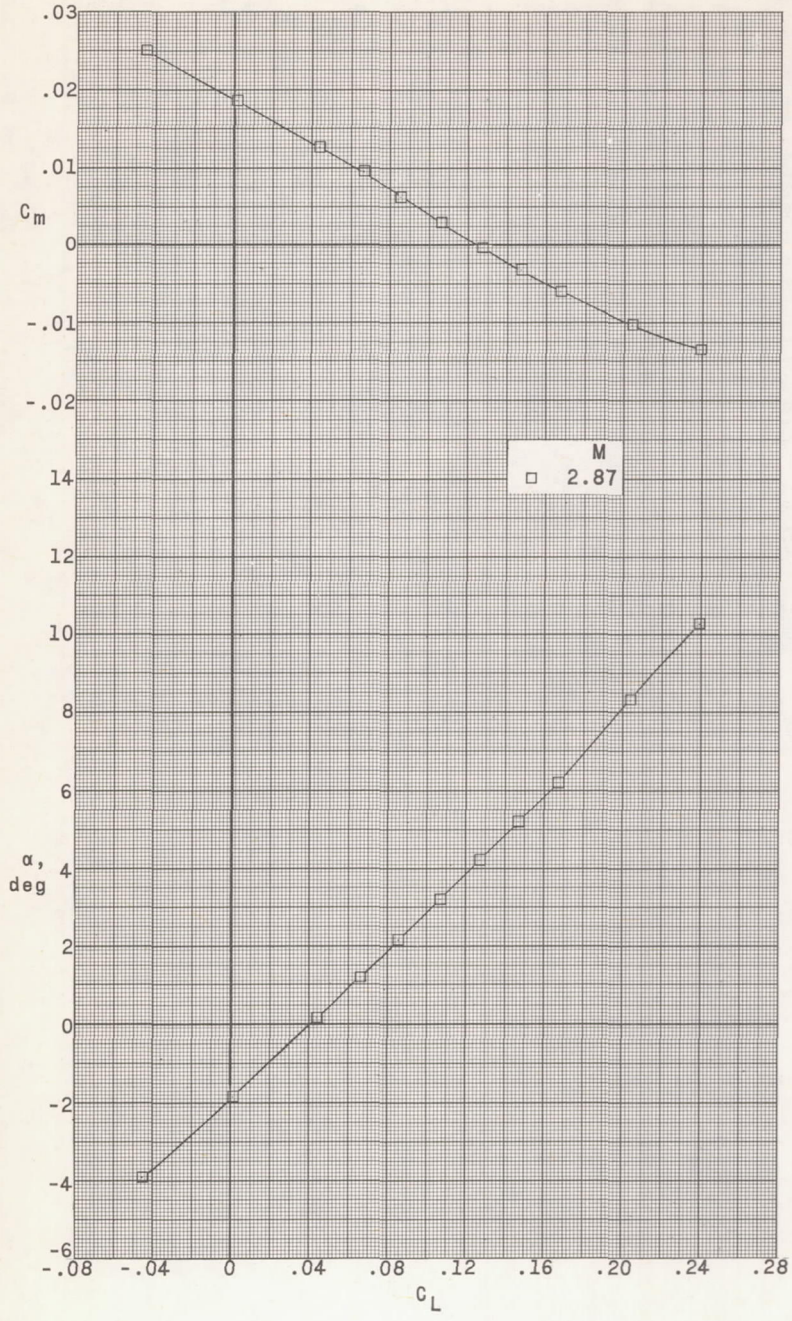

(f) Wing with upper-surface fins and oppositely deflected wing tips. $\delta_{e,L} = -5^\circ$; $\delta_{e,R} = +5^\circ$.

Figure 11.- Continued.

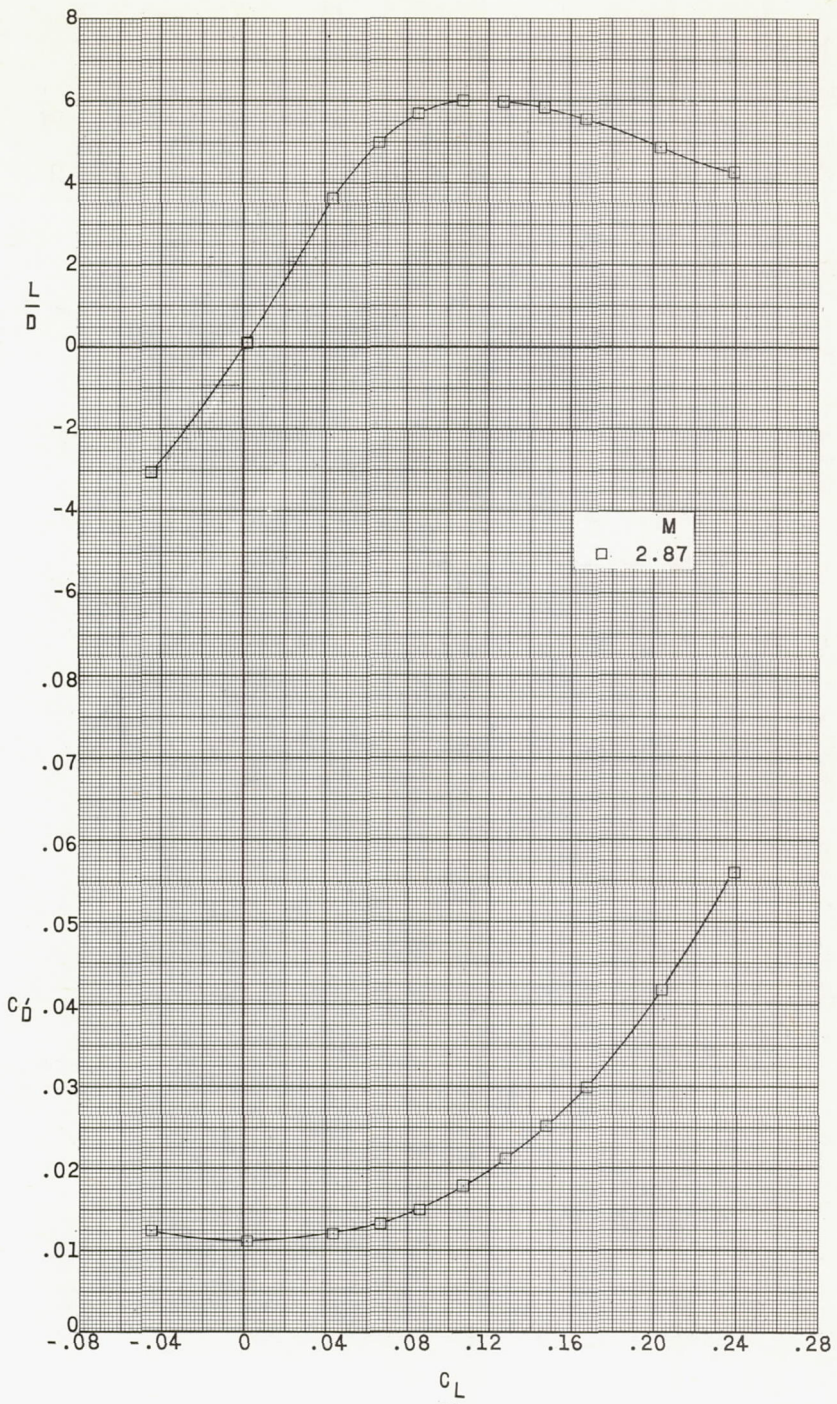

(f) Concluded.

Figure 11.- Continued.

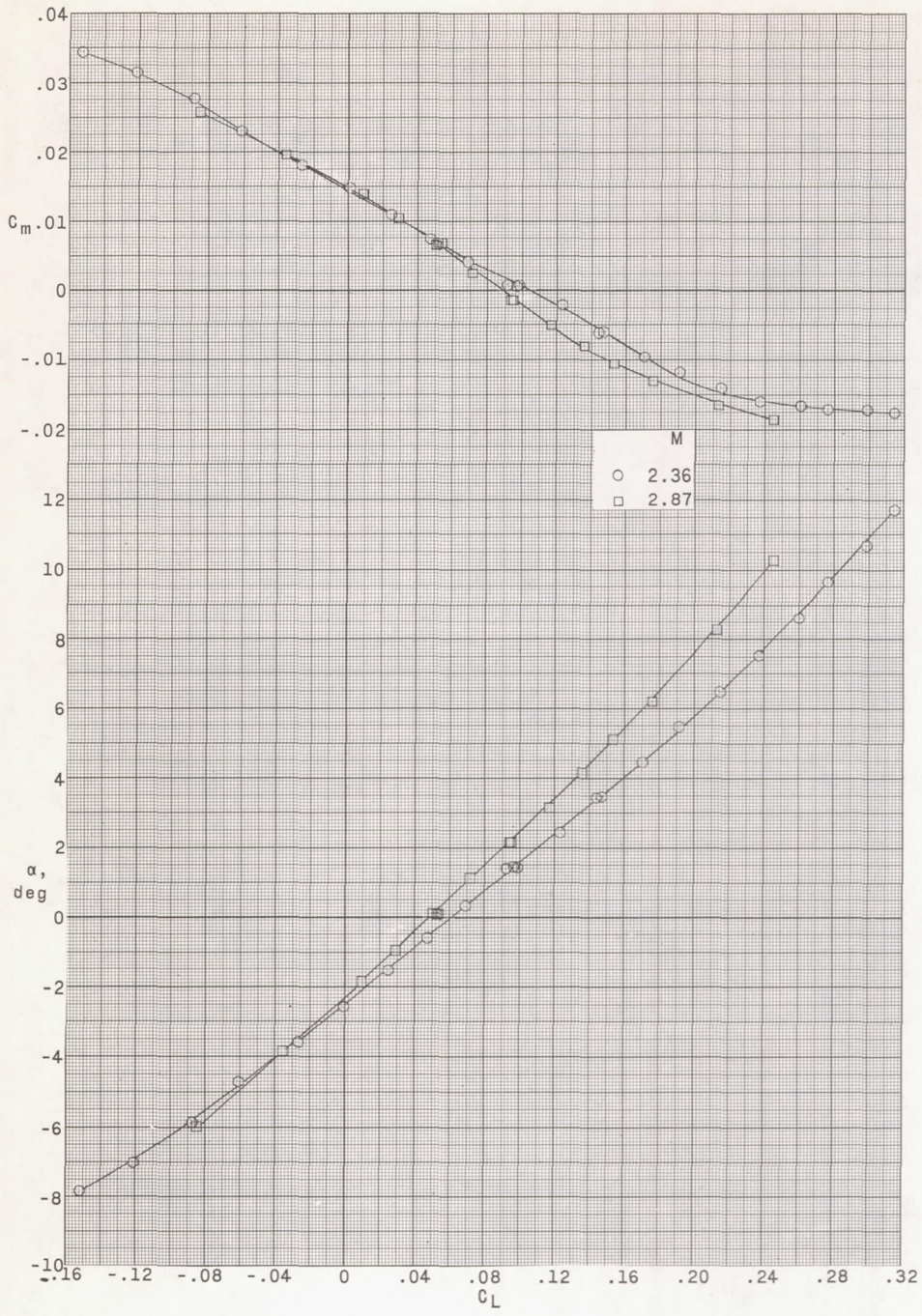

(g) Wing with six underslung pods and upper-surface vertical fins. $\delta_e = 0^o$.

Figure 11.- Continued.

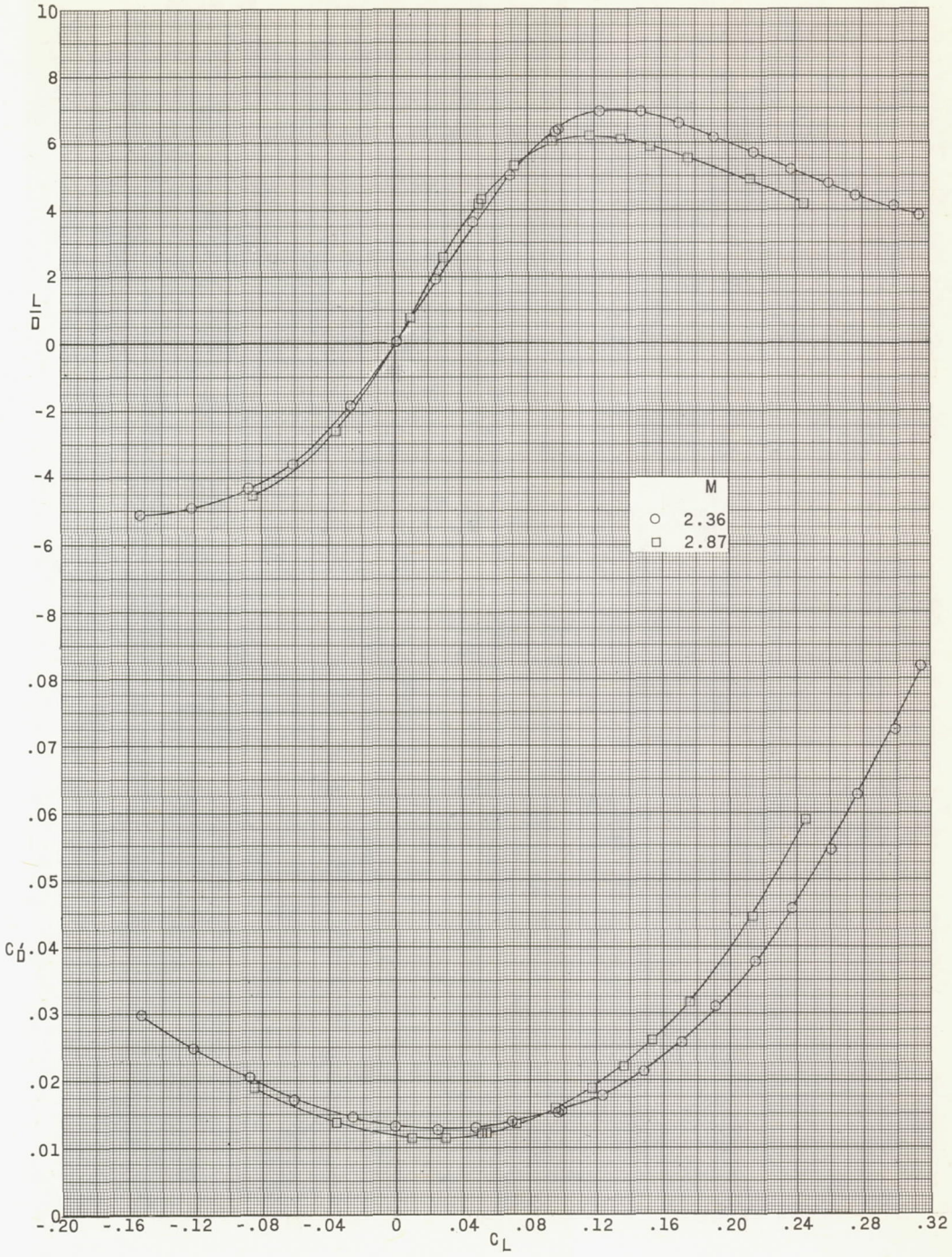

(g) Concluded.

Figure 11.- Continued.

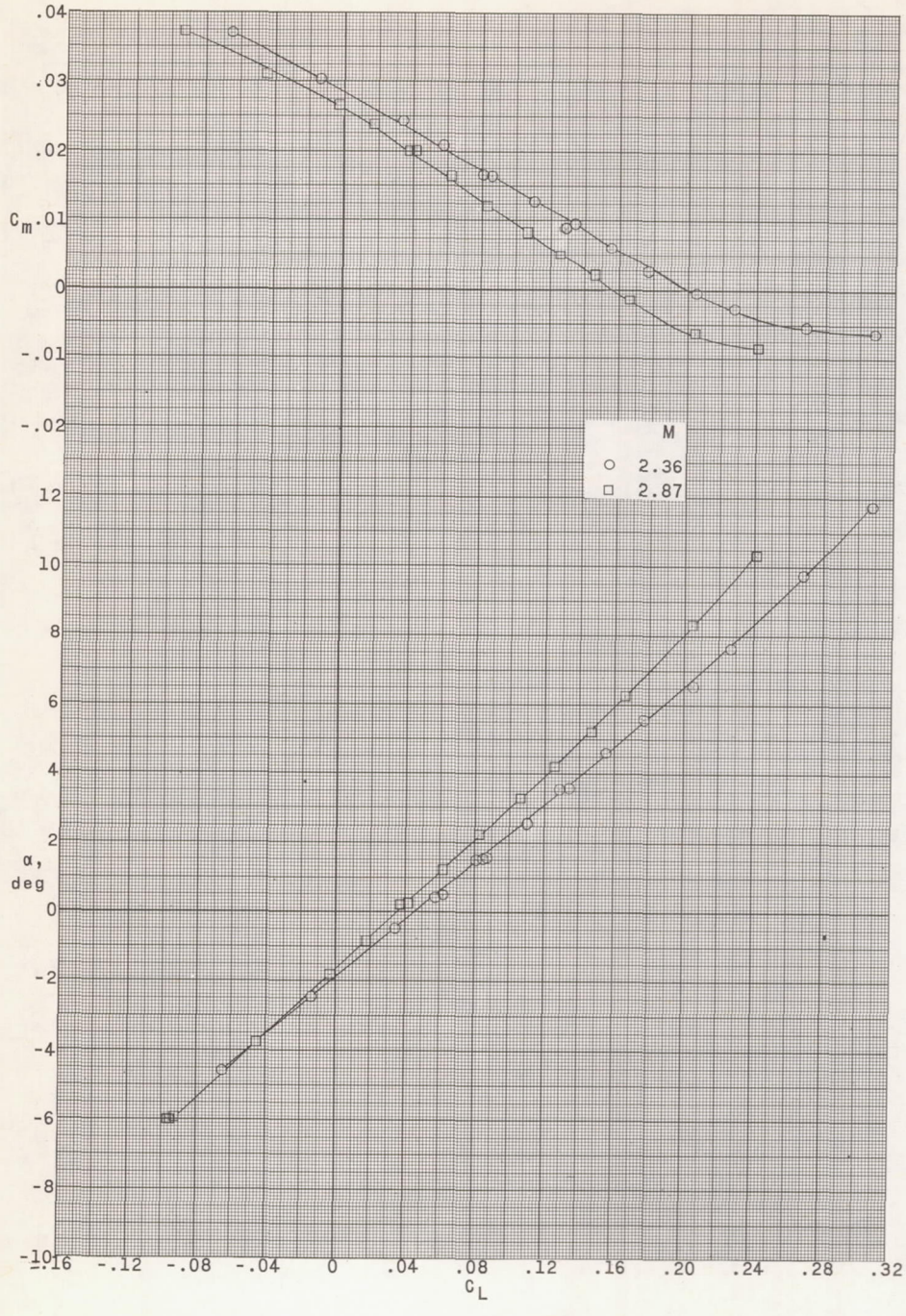

(h) Wing with six underslung pods and upper-surface vertical fins. $\delta_e = -5^\circ$.

Figure 11.- Continued.

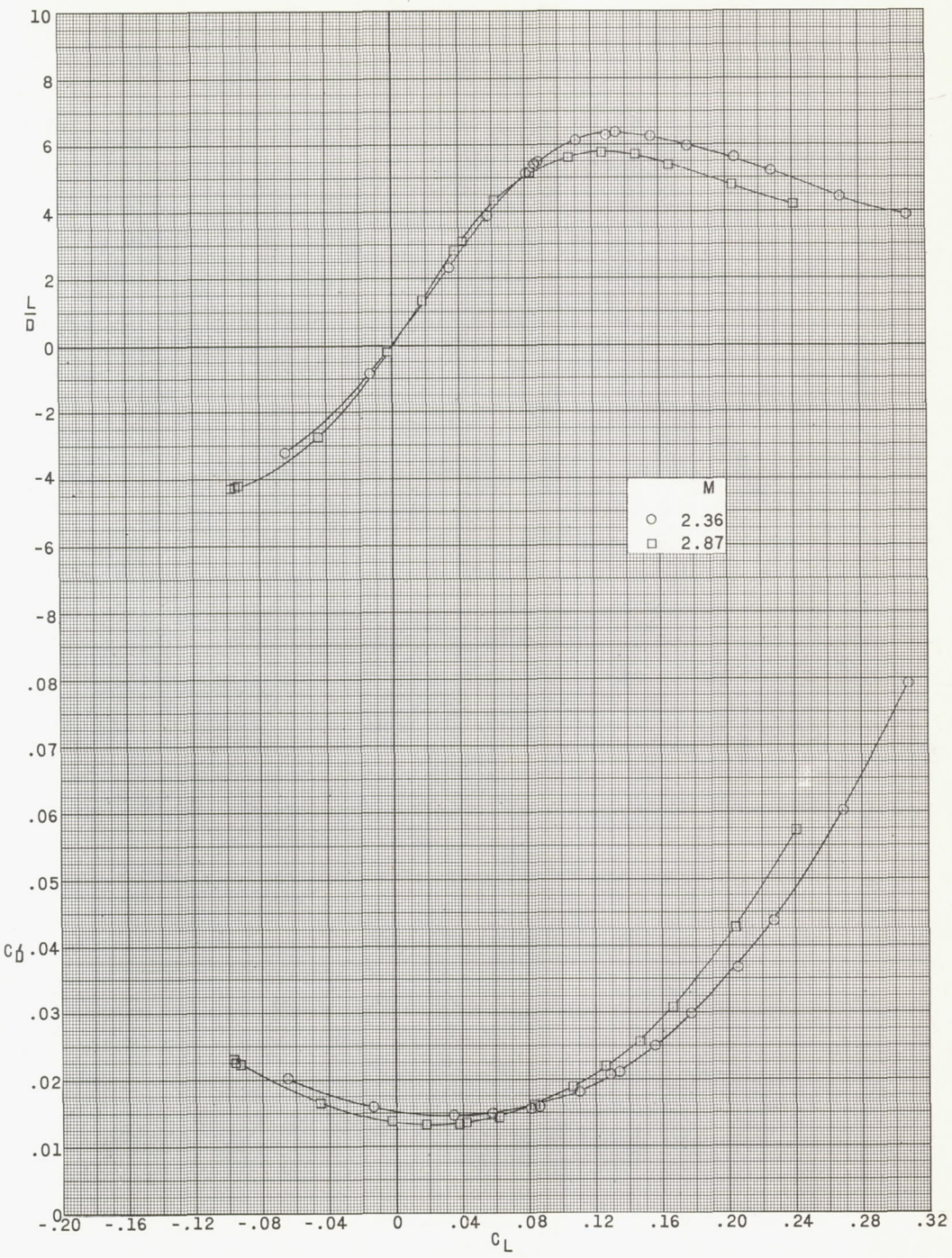

(h) Concluded.

Figure 11.- Continued.

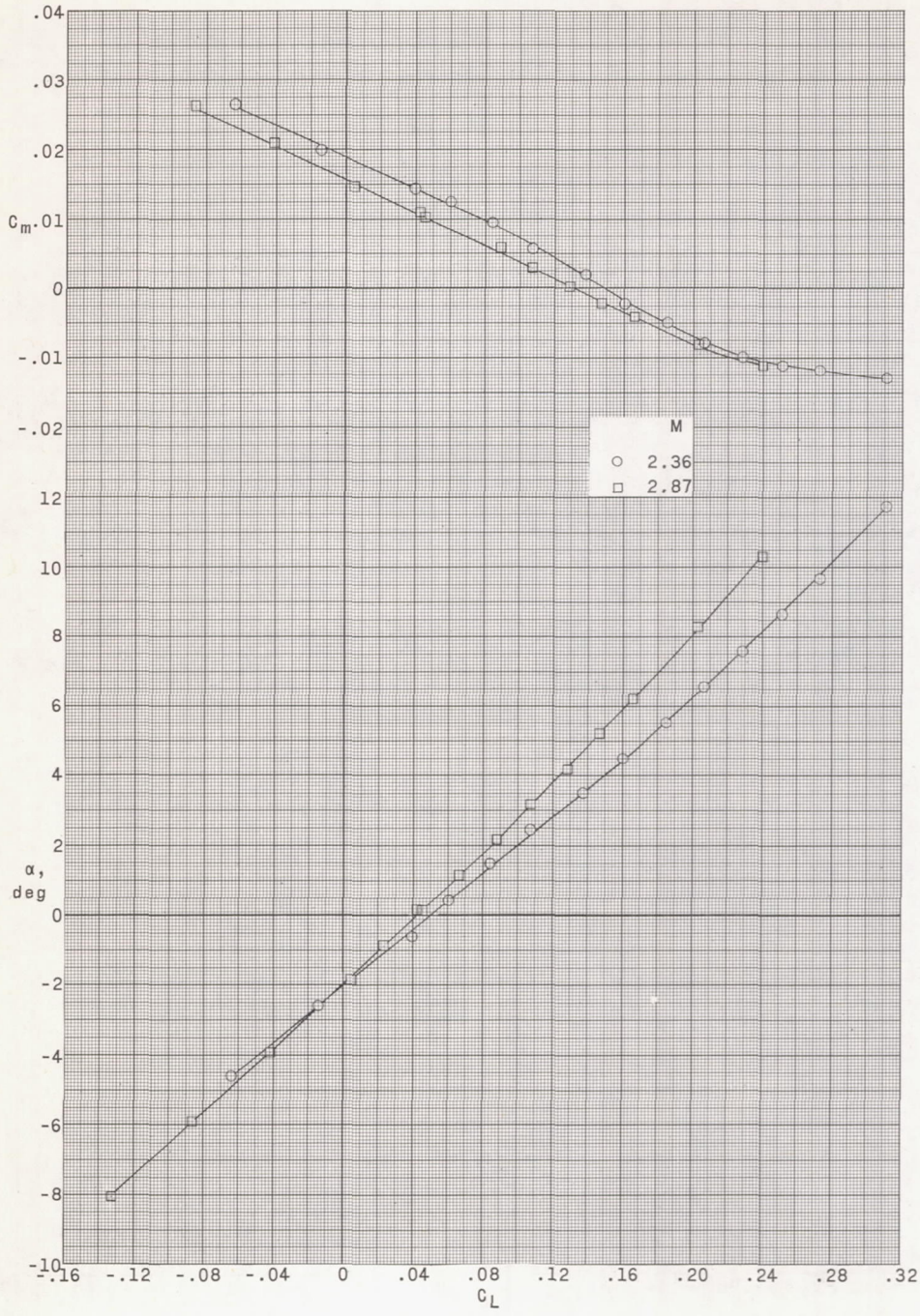

(i) Wing with clustered engine installation with upper- and lower-surface fins. $\delta_e = 0^o$.

Figure 11.- Continued.

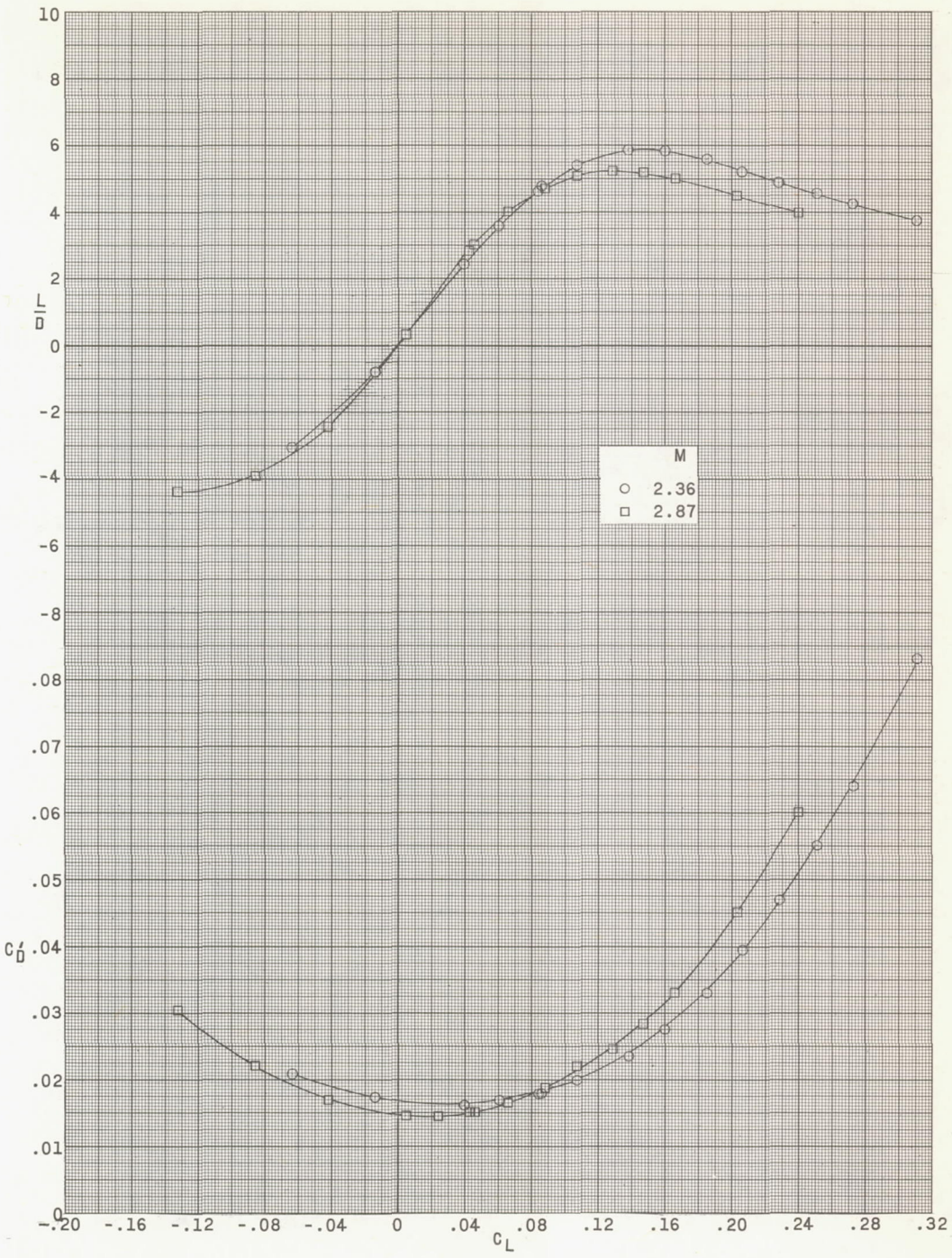

(i) Concluded.

Figure 11.- Concluded.

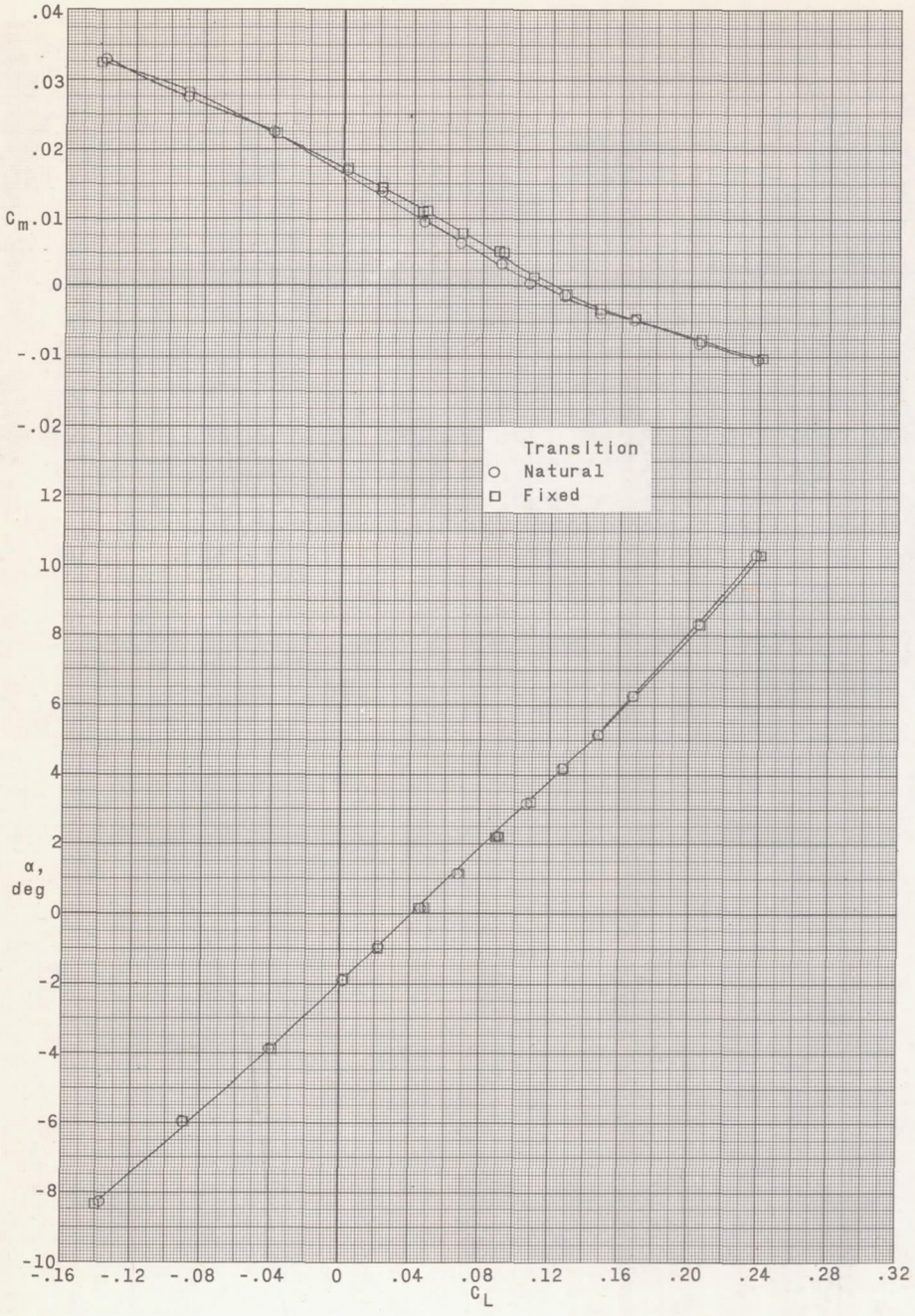

(a) $R = 4.24 \times 10^6$.

Figure 12.- Effects of transition at two Reynolds numbers on pitch characteristics of wing alone at $M = 2.87$.

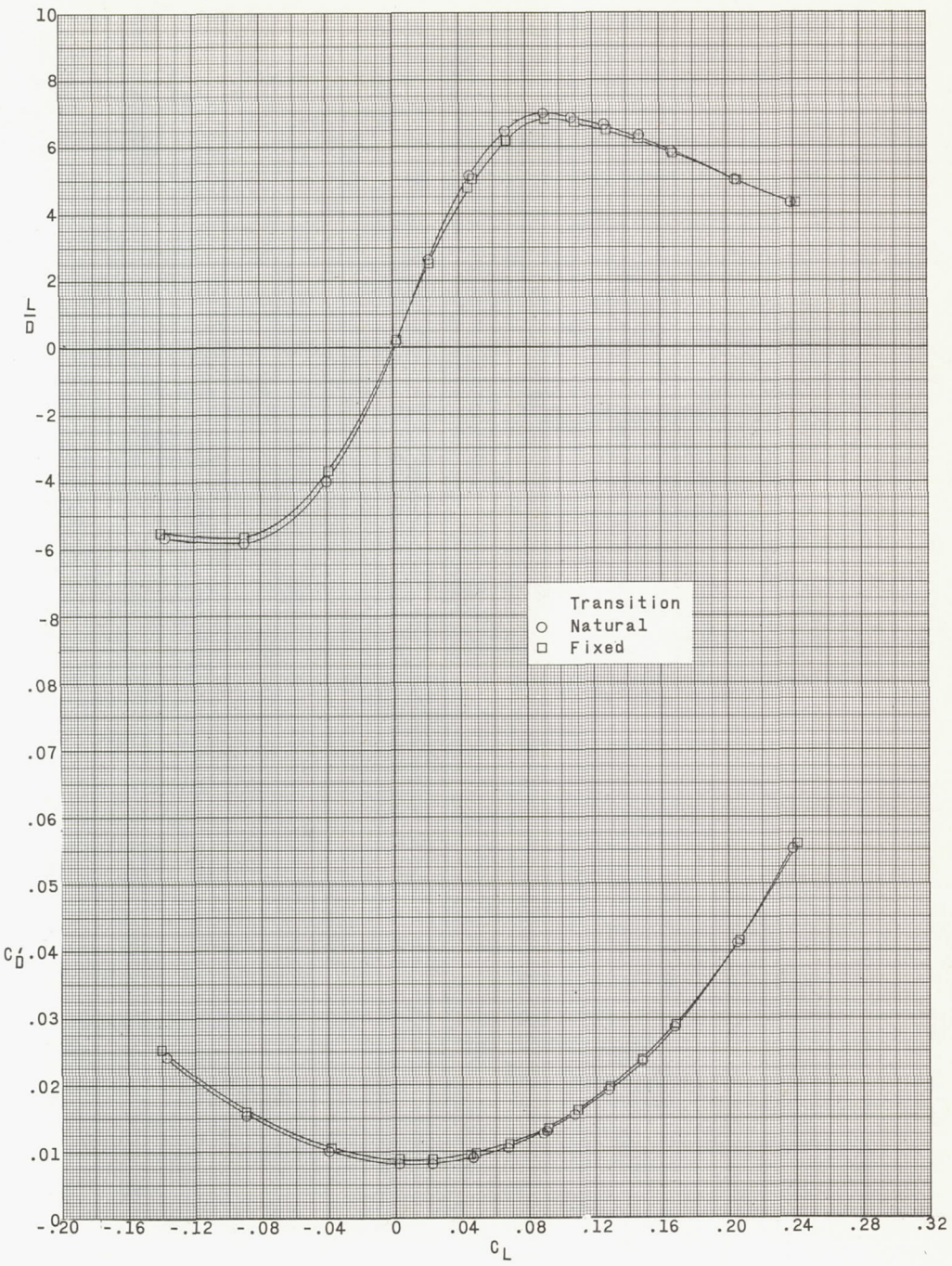

(a) Concluded.

Figure 12.- Continued.

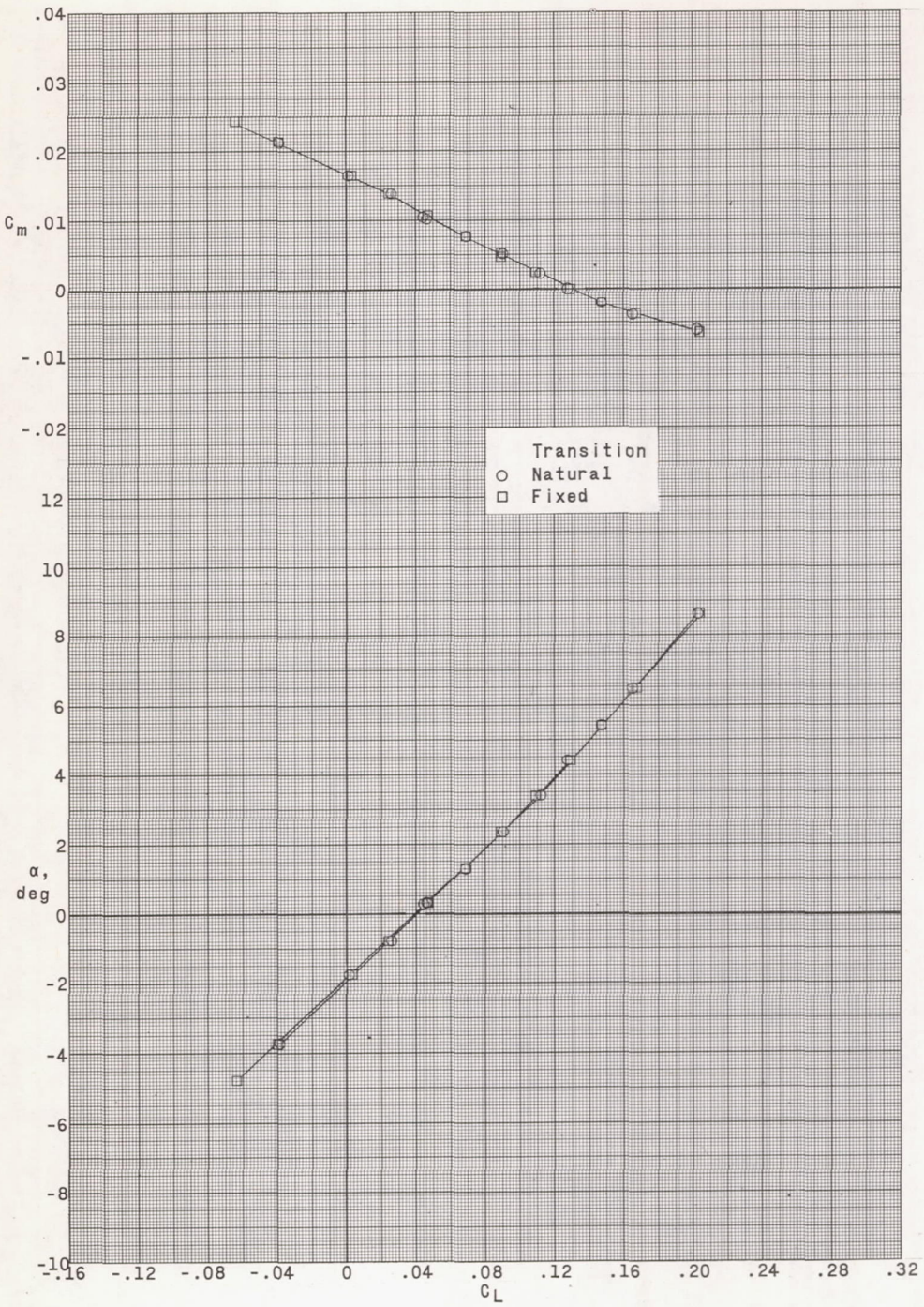

(b) $R = 8.20 \times 10^6$.

Figure 12.- Continued.

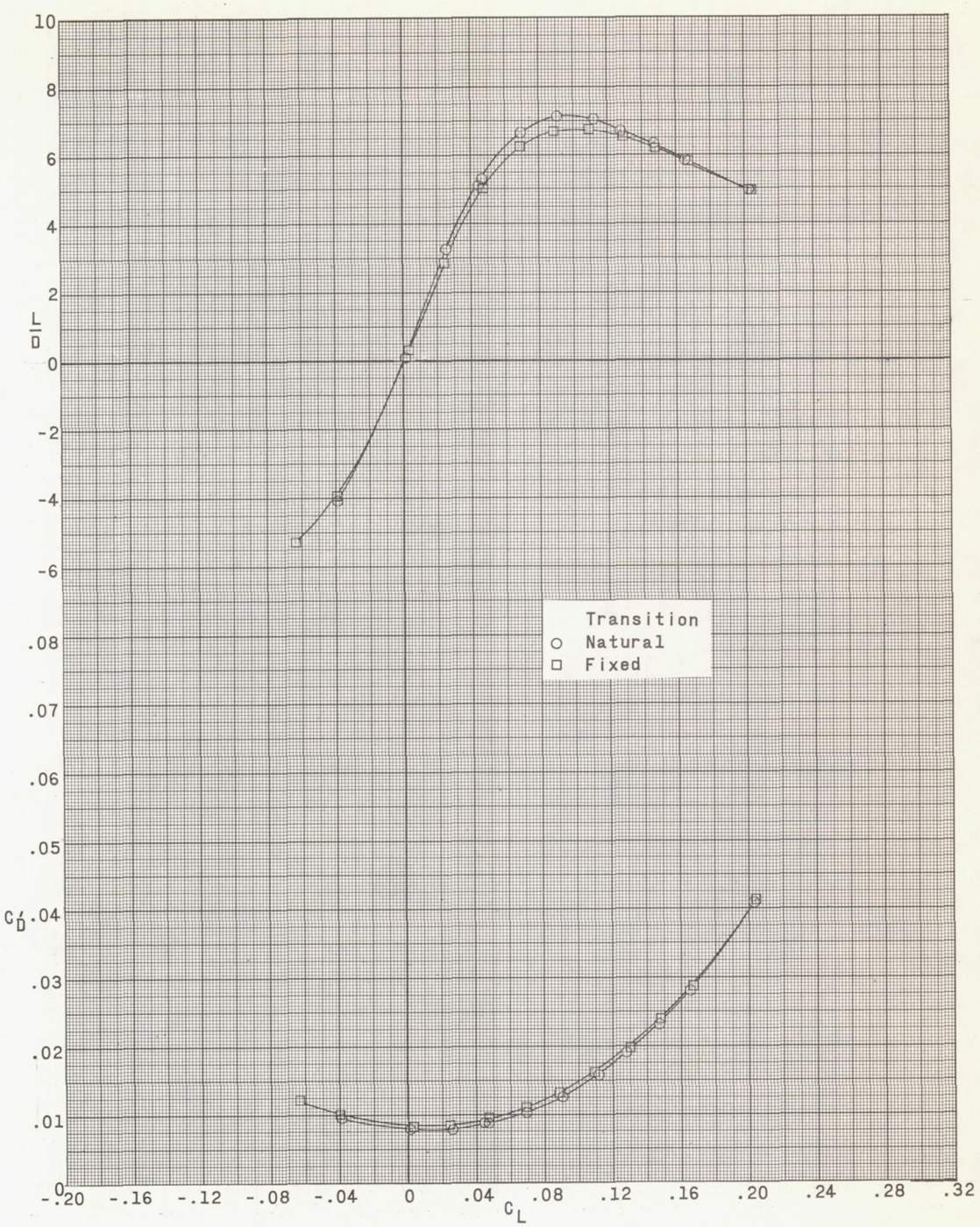

(b) Concluded.

Figure 12.- Concluded.

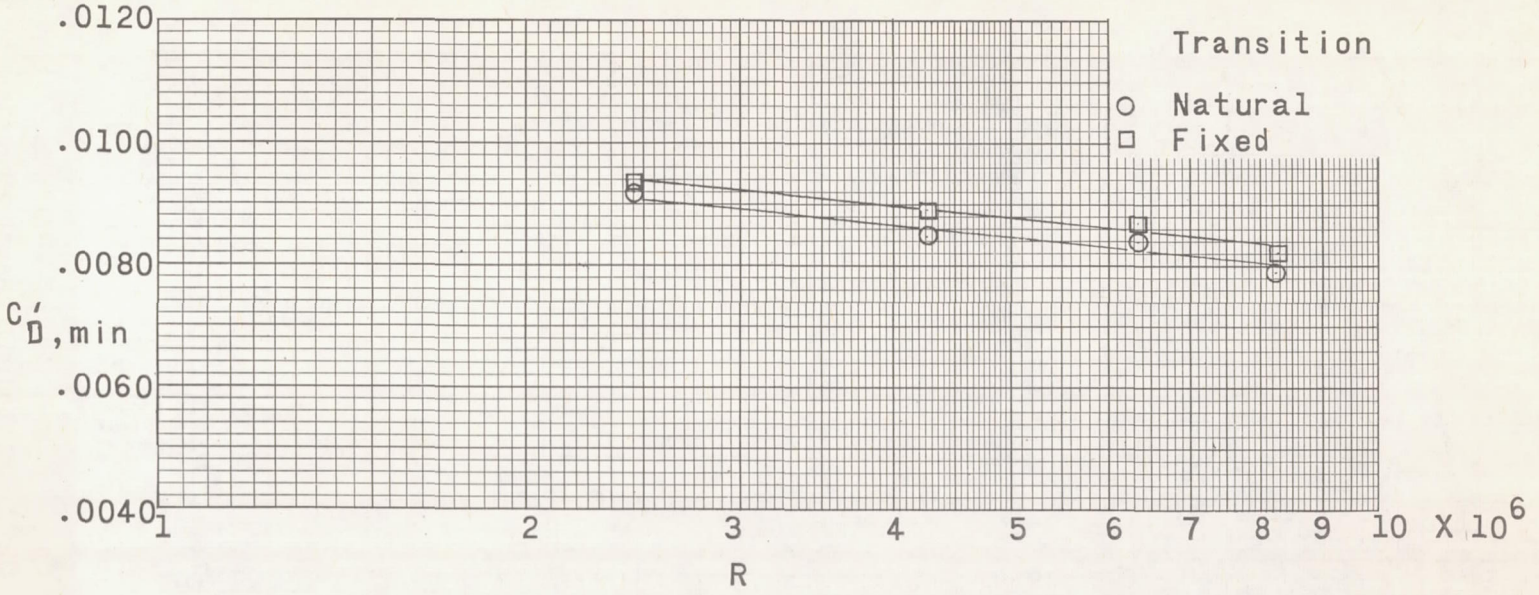

Figure 13.- Variation of $C'_{D,min}$ with Reynolds number for fixed and natural transition on wing alone at a Mach number of 2.87.

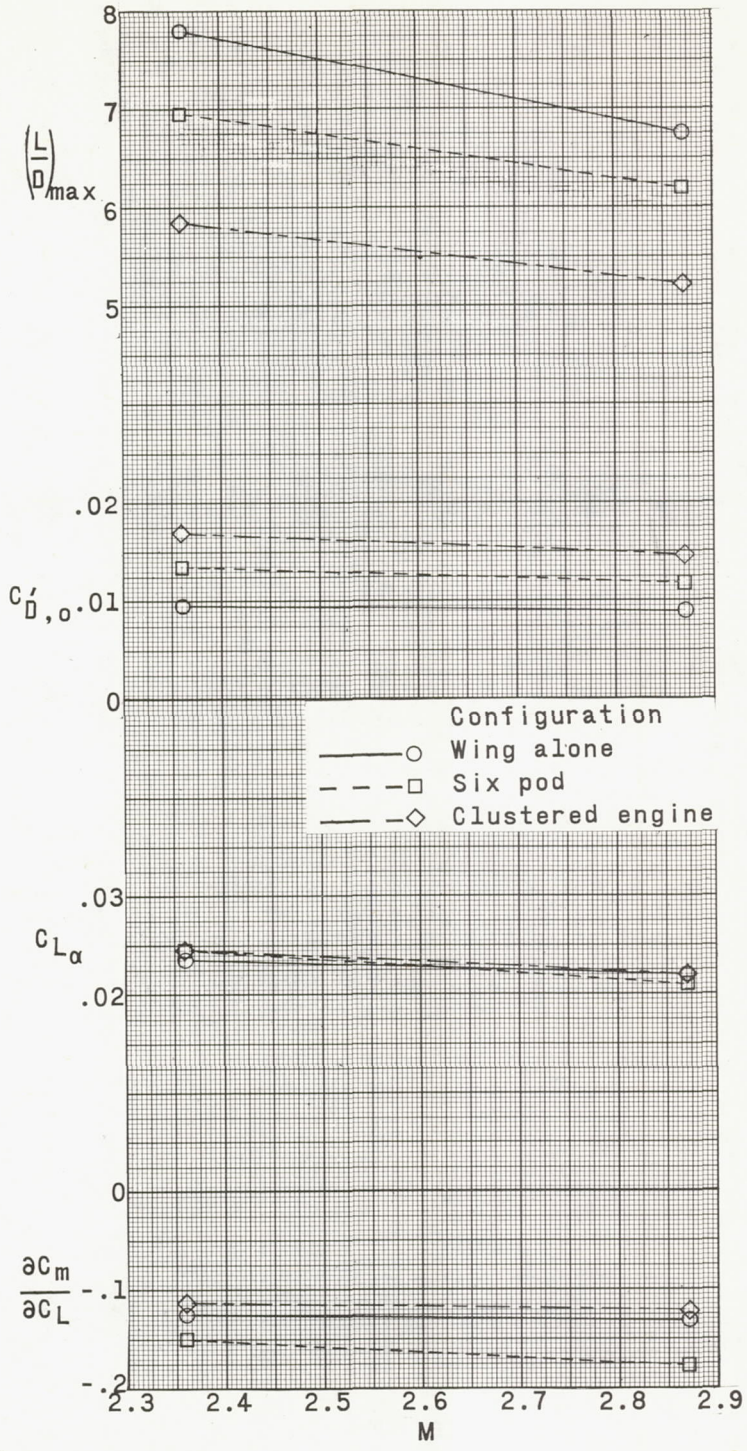

Figure 14.- Summary of the longitudinal characteristics of several model configurations.

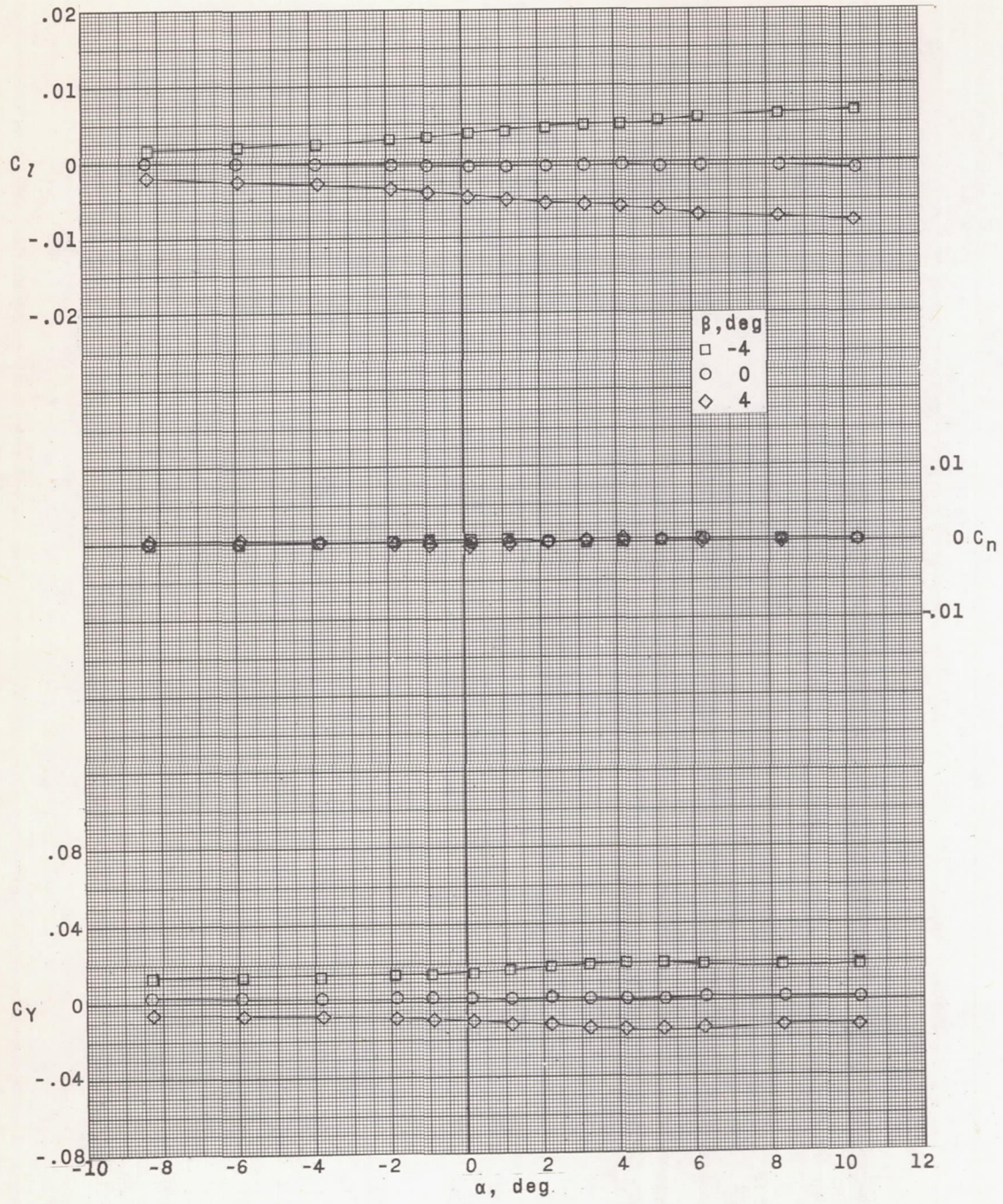

(a) Wing alone.

Figure 15.- Lateral characteristics of the various model configurations at Mach number 2.87.

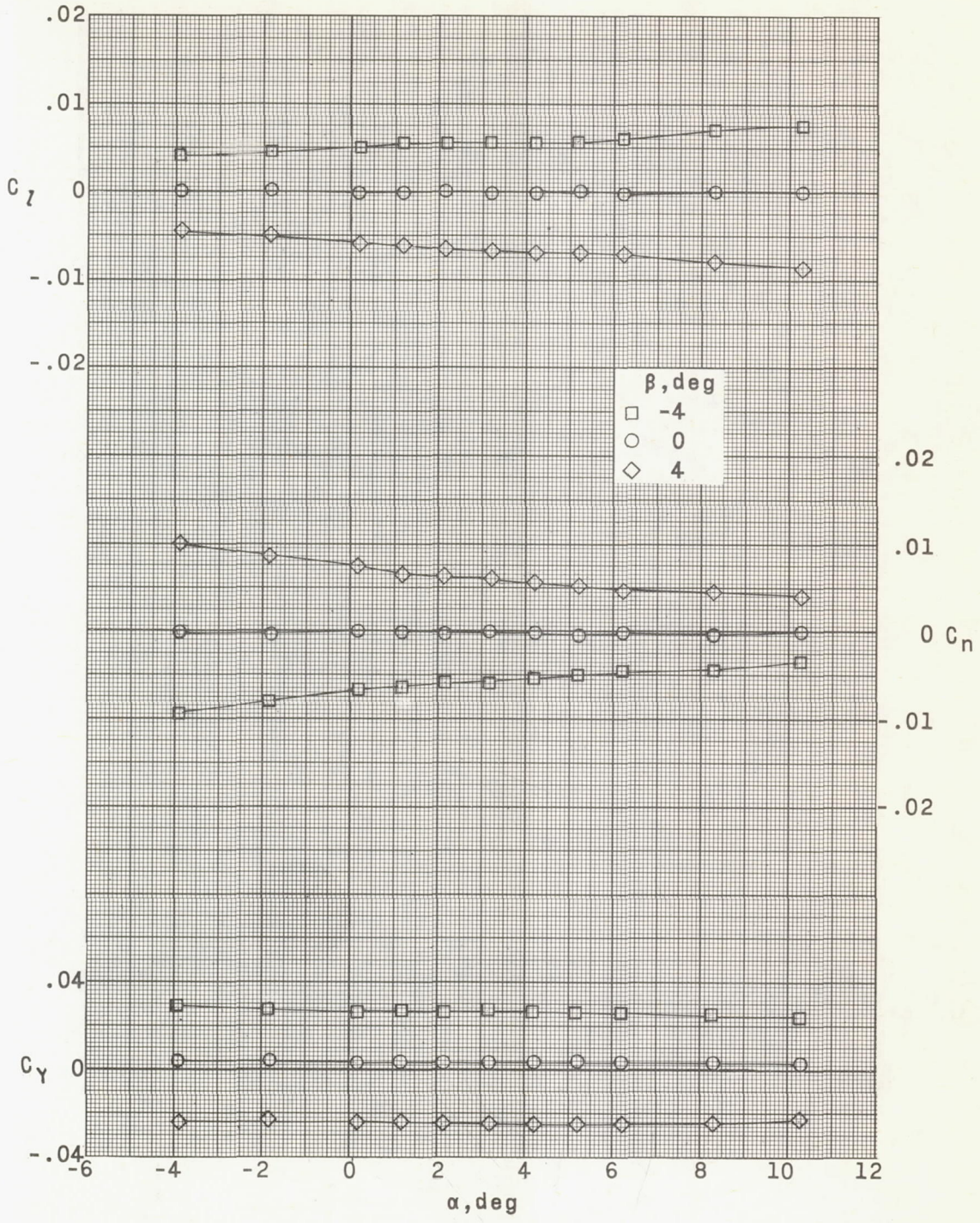

(b) Wing with upper-surface fins. $\delta_r = 0^o$.

Figure 15.- Continued.

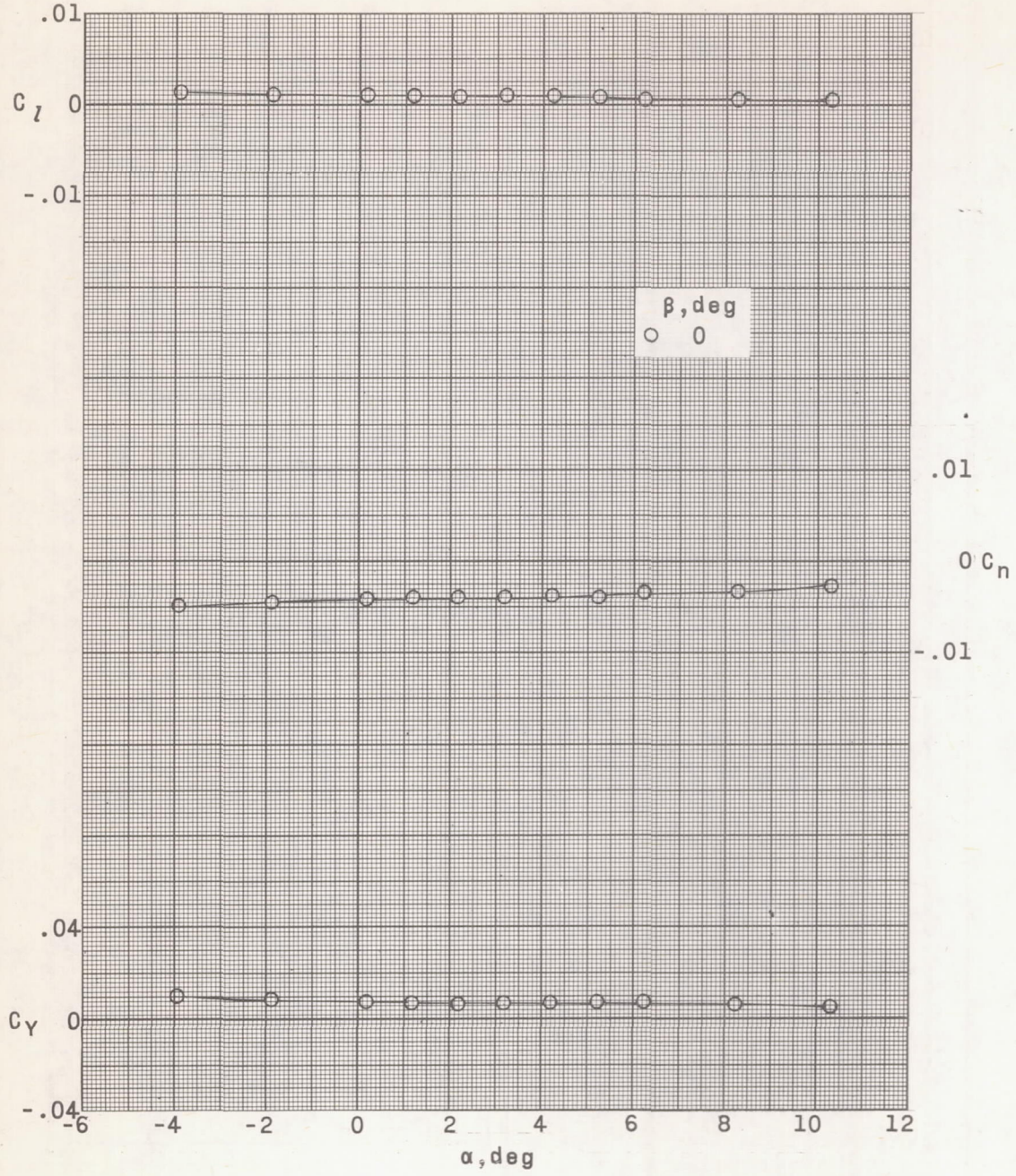

(c) Wing with upper-surface fins deflected. $\delta_r = 5^\circ$.

Figure 15.- Continued.

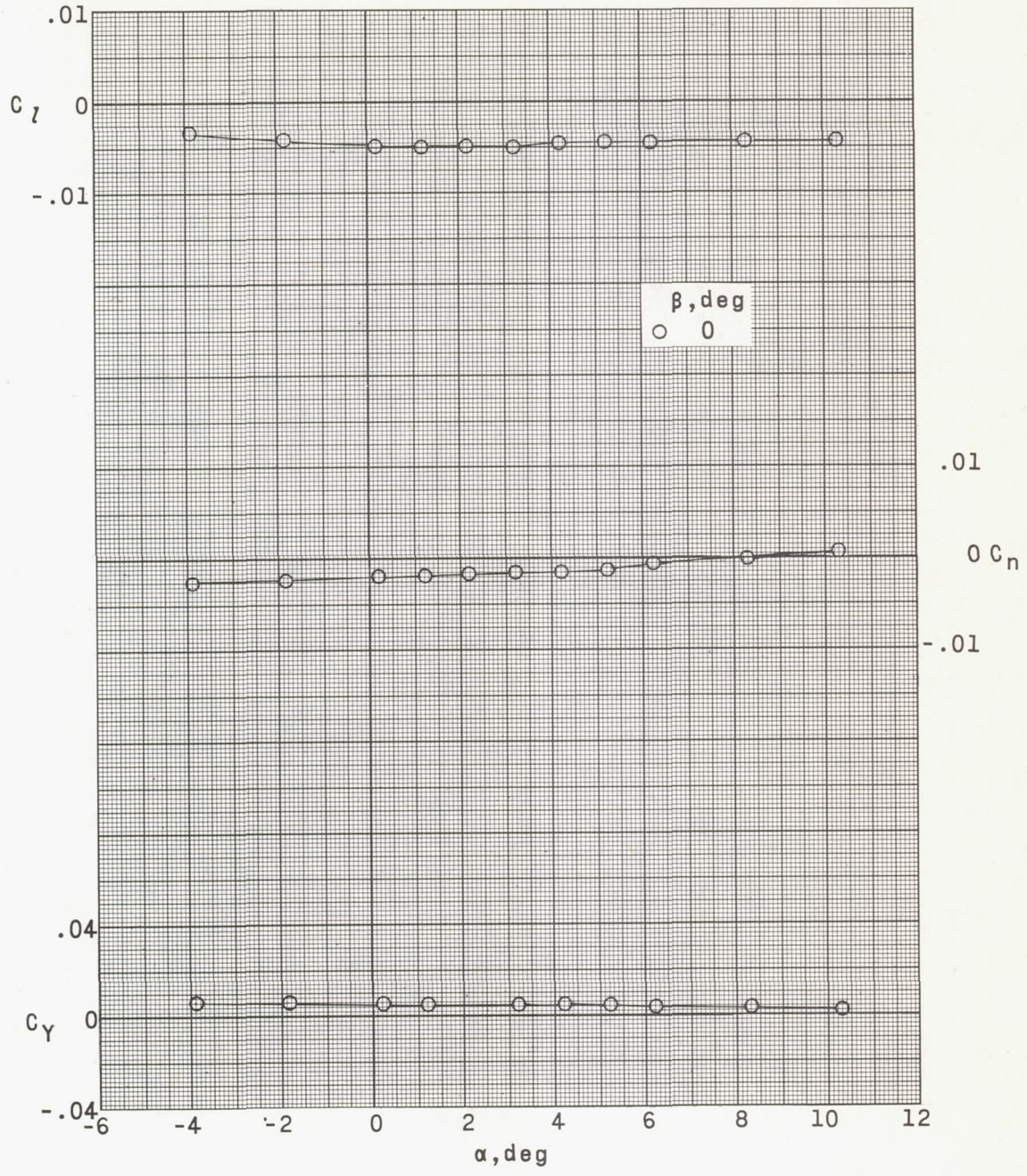

(d) Wing with upper-surface fins and oppositely deflected wing tips. $\delta_{e,L} = -5^{o}$; $\delta_{e,R} = 5^{o}$.

Figure 15.- Continued.

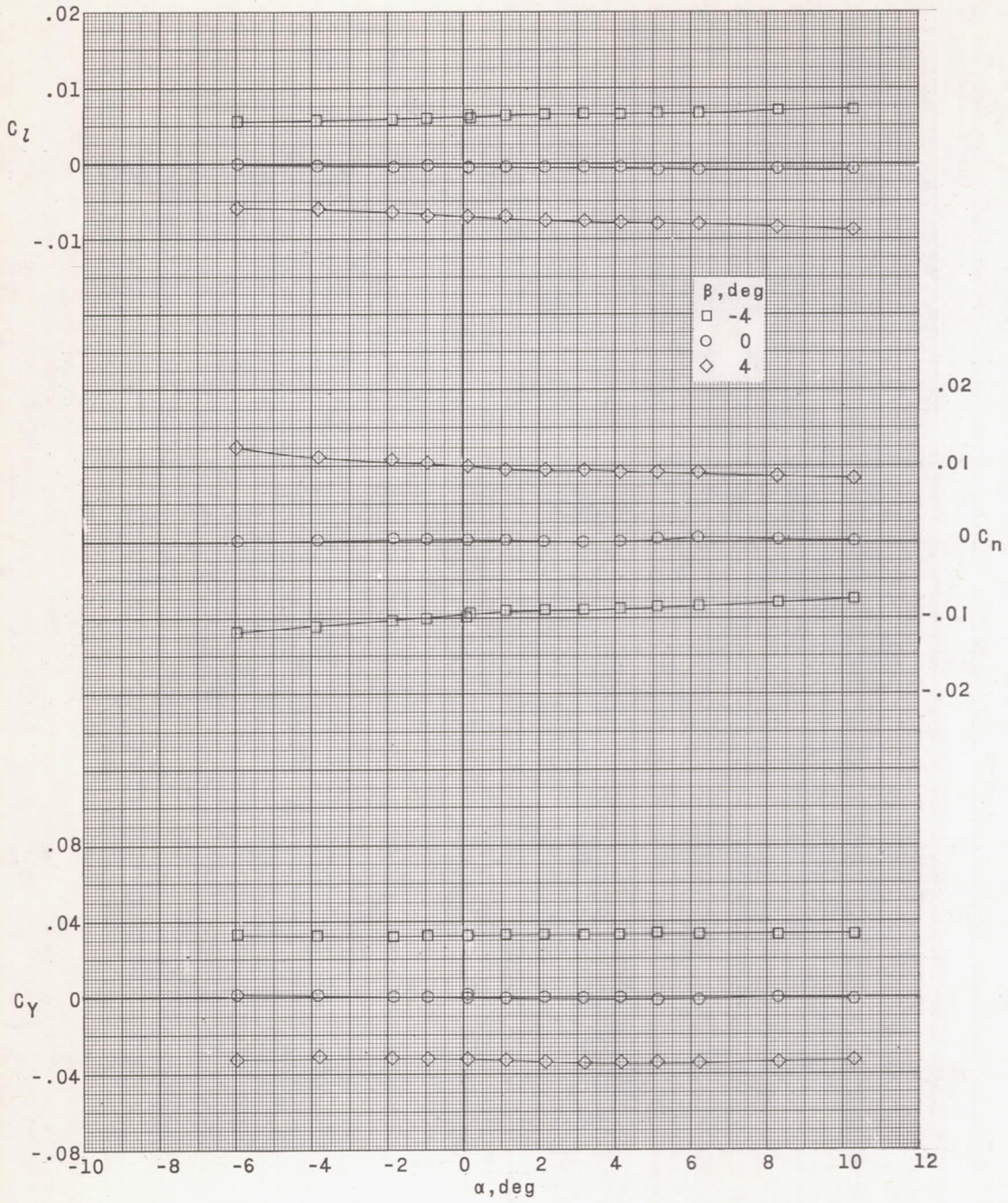

(e) Wing with six underslung pods and upper-surface vertical fins. $\delta_e = 0^o$.

Figure 15.- Continued.

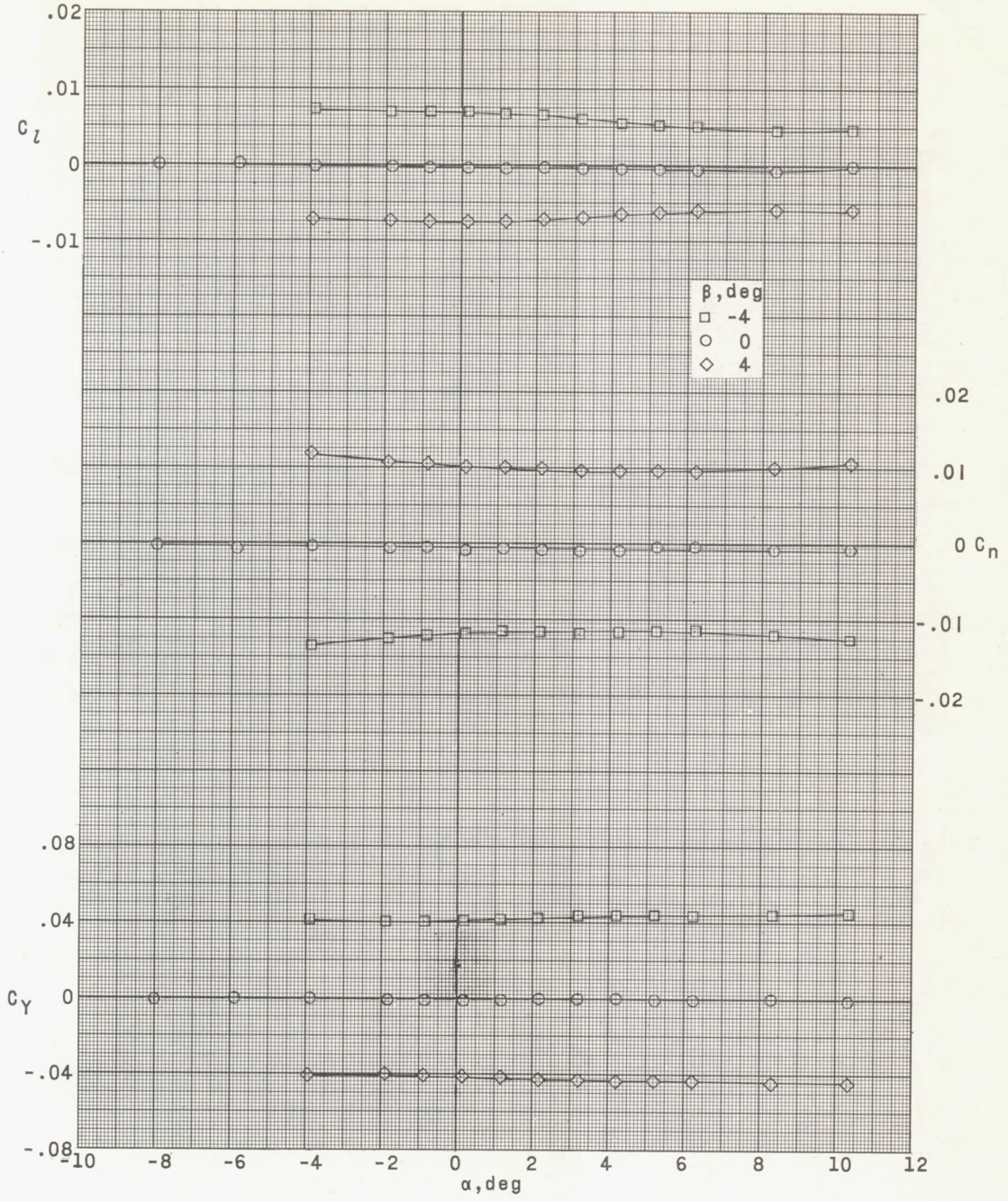

(f) Wing with clustered engine installation with upper- and lower-surface fins. $\delta_e = 0^\circ$.

Figure 15.- Concluded.

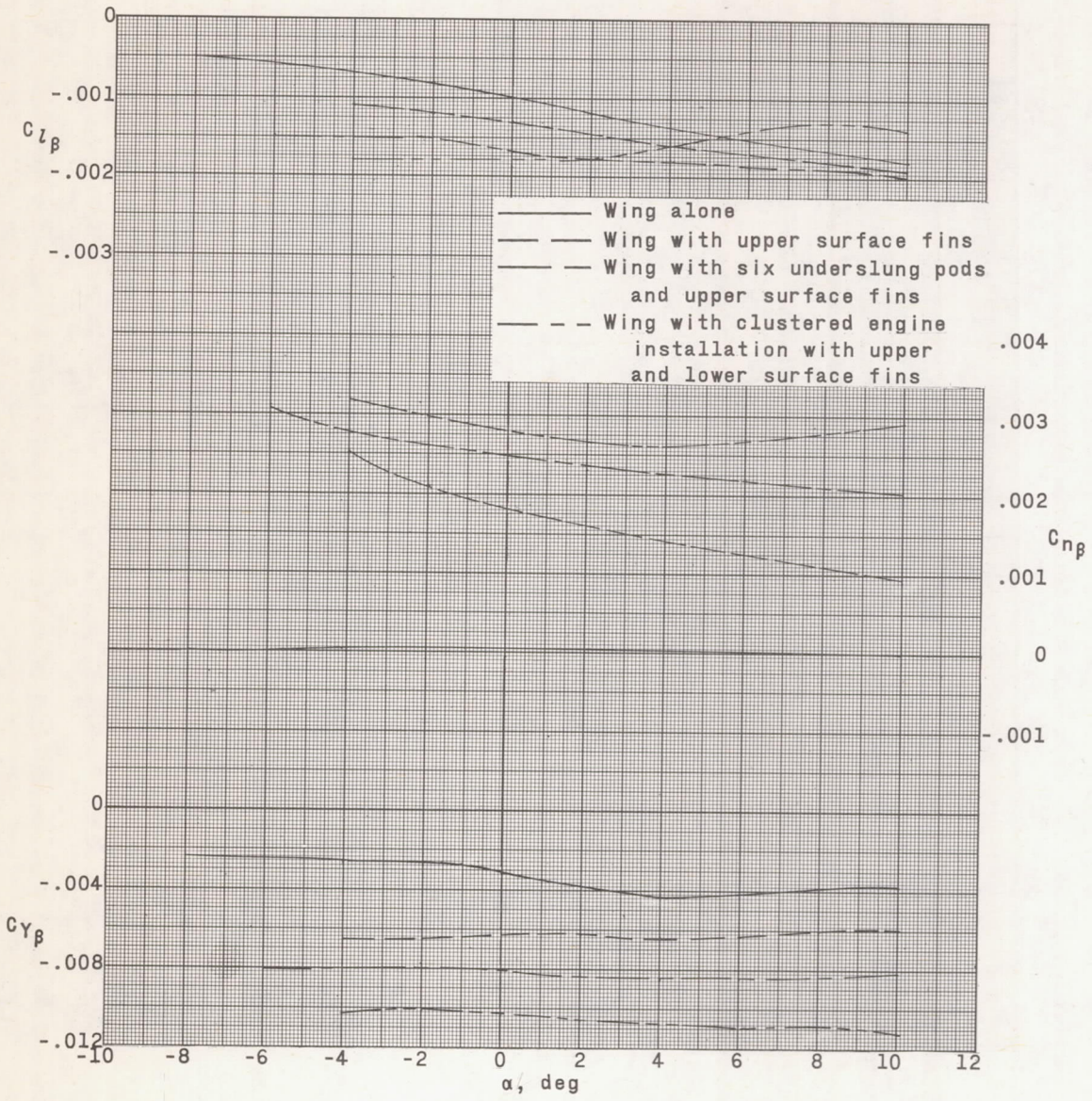

Figure 16.- Sideslip derivatives for several model configurations at Mach number 2.87.